Symmetry Breaking in Density Functional Theory due to Dirac Exchange for a Hydrogen Molecule

Michael Holst [*]   Houdong Hu [†]   Jianfeng Lu [‡]   Jeremy L. Marzuola [§]   Duo Song [¶]

John Weare [‖]

February 12, 2019

Abstract

We study symmetry breaking in the mean field solutions to the 2 electron hydrogen molecule within Kohn Sham (KS) local spin density function theory with Dirac exchange (the XLDA model). This simplified model shows behavior related to that of the (KS) spin density functional theory (SDFT) predictions in condensed and molecular systems. The Kohn Sham solutions to the constrained SDFT variation problem undergo spontaneous symmetry breaking as the relative strength of the non-convex exchange term increases. This results in the change of the molecular ground state from a paramagnetic state to an antiferromagnetic ground states and a stationary symmetric delocalized 1st excited state. We further characterize the limiting behavior of the minimizer when the strength of the exchange term goes to infinity. This leads to further bifurcations and highly localized states with varying character. The stability of the various solution classes is demonstrated by Hessian analysis. Finite element numerical results provide support for the formal conjectures.

1   Introduction

In this paper, we report studies of the properties of density functional theory (DFT) energy minimizers within the context of the hydrogen molecule, (H_2). The (DFT) minimizers discussed are related to those of the Kohn-Sham spin density functional method. The exchange correlation function [48] is simplified by including only Dirac spin density exchange without correlation [48] . We will show that for fixed electron mass, the structure of the minimizing Kohn-Sham solutions change character with the variation of a parameter related to the relative strength of the exchange-correlation component of the functional. Similar studies varying the molecular bond length were undertaken using robust finite element methods for Hartree-Fock and SLDA functionals in [35] and for Hartree-Fock using a maximum overlap method in [7]. The better understanding of such problems is connected to challenges for further developing density functional theory (see e.g., [19, 20]) and directly in the application of density functional theory

---

[*]Department of Mathematics, University of California, San Diego, 9500 Gilman Dr. La Jolla, CA 92093, USA (mholst@math.ucsd.edu).

[†]Microsoft Corporation, Bellevue, WA, USA (vincehouhou@gmail.com).

[‡]Department of Mathematics, Department of Physics, and Department of Chemistry, Duke University, Box 90320, Durham, NC 27708, USA (jianfeng@math.duke.edu).

[§]Department of Mathematics, UNC-Chapel Hill, CB#3250 Phillips Hall, Chapel Hill, NC 27599, USA (marzuola@math.unc.edu).

[¶]Department of Chemistry, University of California, San Diego, 9500 Gilman Dr. La Jolla, CA 92093, USA (dusong@ucsd.edu).

[‖]Department of Chemistry, University of California, San Diego, 9500 Gilman Dr. La Jolla, CA 92093, USA (jweare@ucsd.edu).

(DFT) to highly correlated condensed materials [21] [26] [49] and in spin ordered molecular systems. In addition, uniqueness and symmetry breaking in other quantum mechanical models have recently been studied widely in for instance the works [24, 25] for polaron models, [31, 29, 30] for Hartree-Fock models of atoms, and many others. A similar strategy to that undertaken here in one of our limits was explored for the periodic Thomas–Fermi–Dirac–von Weizsäcker model in [52, 53].

We consider a neutral hydrogen molecule (H_2) with nuclei placed $2R$ apart. The external potential is given by (after a possible coordinate change)

$$V_R(x) = -\frac{1}{|x_i - Re_1|} - \frac{1}{|x_i + Re_1|}, \tag{1}$$

where e_1 is the $(1,0,0)$ vector in $\mathbb{R}^3$ and x_1 and x_2 denote the positions of the two electrons and we use atomic units. The two-electron Schrödinger operator is given by

$$H_2 = -\frac{1}{2}\Delta_{x_1} - \frac{1}{2}\Delta_{x_2} + V_R(x_1) + V_R(x_2) + \frac{1}{|x_1 - x_2|}. \tag{2}$$

In this work, we will consider the spin-polarized density functional theory with the exchange energy taken to be Dirac exchange and without correlation energy. In the literature, the spin free version of this model is sometimes referred as the XLDA model. We are interested in the spin paired ground state of the system with spin up ψ_+ and spin down ψ_- spatial wave functions. We would like to study the impact of the exchange term on the electronic structure. Therefore, we introduce a strength parameter α for the exchange-correlation energy. The DFT energy functional is hence given by

$$\mathcal{E}_\alpha(\psi_+, \psi_-) = \frac{1}{2}\int |\nabla\psi_+|^2 \, dx + \frac{1}{2}\int |\nabla\psi_-|^2 \, dx + \int V_R(x)\rho(x) \, dx$$
$$+ \frac{1}{2}\iint \frac{\rho(x)\rho(y)}{|x-y|} \, dx \, dy - \alpha \int \left(|\psi_+|^{8/3} + |\psi_-|^{8/3} \right) dx, \tag{3}$$

where the electron density of the system is given by

$$\rho(x) = |\psi_+(x)|^2 + |\psi_-(x)|^2. \tag{4}$$

Note in particular in (3) the Dirac exchange term is spin-polarized: let $\rho_\pm = |\psi_\pm|^2$, the exchange term is given by

$$-\alpha \int \left(\rho_+^{4/3} + \rho_-^{4/3} \right) dx \tag{5}$$

as exchange effect originated from Pauli's exclusion principle only occurs between electrons with same spin polarization.[48] [46]

The H_2 molecule has reflection symmetry. We are interested in the symmetry (delocalization) (or lack of symmetry, localization) of ψ_+ and ψ_-. We call the minimizer with the symmetry constraint, $\psi_+ = \psi_- = \psi_R$, a restricted minimizer to the energy functional, denoted as ψ_R. Thus

$$\psi_R = \arg\min \mathcal{E}_\alpha(\psi, \psi)$$
$$\text{s.t.} \quad \int |\psi|^2 = 1. \tag{6}$$

The unrestricted minimization on the other hand considers all possible ψ_+ and ψ_- with the normalization constraints. To distinguish, we denote the minimizers as $\psi_\pm$.

$$(\psi_+, \psi_-) = \arg\min E_\alpha(\psi_+, \psi_-)$$
$$\text{s.t.} \quad \int |\psi_+|^2 = \int |\psi_-|^2 = 1. \tag{7}$$

Our goal in this work is to understand the symmetry breaking, i.e., the question whether $\psi_+ = \psi_- = \psi_R$. The following result gives the existence of minimizers to both (6) and (7).

Proposition 1.1. *For all $\alpha \geq 0$, there exist solutions $(\phi_+, \phi_-) \in H^1 \times H^1$ with $\int |\phi_\pm|^2 \, dx = 1$ such that*

$$\mathcal{E}_\alpha(\phi_+, \phi_-) = \min_{\psi_\pm \in H^1; \int |\psi_\pm|^2 dx = 1} \mathcal{E}_\alpha(\psi_+, \psi_-).$$

For a proof of this proposition, we refer the reader to the Concentration Compactness tools employed in [3, Theorem 1] or specifically for LDA models the recent work of [28], where a general existence theory is addressed for LDA models of this type with neutral or positive charge.

For the energy functional (3), we have two parameters R and α in the functional. We expect the following behavior of the minimizers for different ranges of parameters:

1. For $\alpha = 0$ and any $R > 0$, the minimizer have the symmetry $\psi_+ = \psi_- = \psi_R$.

2. Fix $R \geq 0$, when we increase α from 0: The minimizer is initially symmetric (hence it is continuous at $\alpha = 0$), the symmetry is broken for larger α ($\psi_+ \neq \psi_-$). The critical parameter α for the transition from symmetric to asymmetric minimizer depends on R.

3. Fix $\alpha > 0$, for R sufficiently large, the minimizer is asymmetric.

Therefore, this suggests a two-dimensional phase diagram where the axes are R and α with a phase transition from symmetric to asymmetric minimizers. In the current manuscript, we will fix R and vary the parameter α in our analysis. However, we will demonstrate the (α, R) phase diagram numerically. Some technical difficulties arise in the the analysis when varying R, which we comment on in Section 5 and plan to address in future work. We make our statements precise in the following theorems.

Theorem 1. *Fix $R > 0$, denote ψ_R the minimizer of (6) and $\psi_\pm$ the minimizer of (7), we have $\psi_\pm = \psi_R$ for $\alpha \ll 1$, and $\psi_+ \neq \psi_-$ for $\alpha \gg 1$.*

In other words, as we increase α, the symmetry $\psi_+ = \psi_-$ is broken. In fact, we can give a more precise characterization of the minimizer $\psi_\pm$ as $\alpha \to \infty$.

Theorem 2. *Fix $R > 0$, as $\alpha \to \infty$, the rescaled and translated minimizer of (7)*

$$\alpha^{-\frac{3}{2}} \psi_\pm(\alpha^{-1}(x \mp R e_1))$$

converges to ϕ in H^1, where ϕ is the unique positive, radial solution to the equation

$$-\frac{1}{2}\Delta\phi - \frac{4}{3}|\phi|^{\frac{2}{3}}\phi + E\phi = 0, \text{ with } \int |\phi|^2 dx = 1. \tag{8}$$

This can also be seen as the constrained minimizer of the Lagrangian

$$\mathcal{E}_s(\phi) = \frac{1}{2}\int |\nabla\phi|^2 \, dx - \int |\phi|^{8/3} \, dx, \tag{9}$$

with mass $\int |\phi|^2 \, dx = 1$. In other words, as $\alpha \to \infty$, each electron becomes concentrated over a different nucleus.

Our results in the small α setting rely heavily on the results of Lieb, Lions and others relating to the concentration compactness phenomenon for constructing minimizers of constrained Lagrangians at $\alpha = 0$, then an application of the Implicit Function Theorem for α small. Our result for large α on the

3

other hand follows from essentially comparing the variational problem to a scale-invariant semi-linear problem, which in turn relies strongly on the orbital stability of solitons for the unperturbed Dirac non-linearity in 3 dimensions, $|u|^{\frac{2}{3}}u$.

The proof for the small α regime is presented in Section 2, while the large α regime is treated in Section 3. We present the analysis in detail for fixed $R > 0$ and varying α throughout the proof. Without of loss of generality, for our analysis we will assume $R = 1$ and denote $V = V_R$. Detailed numerical studies of the (α, R) phase diagram and in particular the transition between small and large α for fixed R are discussed in Section 4. Concluding remarks and a discussion of the analysis in case of varying R is included in Section 5. The numerical methods are presented in Appendix A using a finite element package developed by the group of the first author and developed in the thesis of the second author to study variational problems in electronic structure.

2 Proof in the small α regime

2.1 The restricted Hartree model: Case $\alpha = 0$

When $\alpha = 0$, the energy functional we consider becomes

$$\mathscr{E}_0(\psi_+, \psi_-) = \frac{1}{2}\int |\nabla\psi_+|^2\,\mathrm{d}x + \frac{1}{2}\int |\nabla\psi_-|^2\,\mathrm{d}x + \int V(x)\rho(x)\,\mathrm{d}x + \frac{1}{2}\iint \frac{\rho(x)\rho(y)}{|x-y|}\,\mathrm{d}x\,\mathrm{d}y. \tag{10}$$

Without the exchange-correlation energy, the minimizer is always symmetric. Indeed, fixing any density ρ with $\int \rho = 2$, we have

$$\mathscr{E}_{\mathrm{LDA},0}(\sqrt{\rho}/\sqrt{2}, \sqrt{\rho}/\sqrt{2}) = \inf\{E_{\mathrm{LDA},0}(\psi_+, \psi_-)\,|\,|\psi_+|^2 + |\psi_-|^2 = \rho\}. \tag{11}$$

Define $\rho_+ = |\psi_+|^2$ and $\rho_- = |\psi_-|^2$, the above follows from the convexity

$$2\int \left|\nabla\sqrt{(\rho_+ + \rho_-)/2}\right|^2\,\mathrm{d}x \leq \int |\nabla\sqrt{\rho_+}|^2\,\mathrm{d}x + \int |\nabla\sqrt{\rho_-}|^2\,\mathrm{d}x, \tag{12}$$

and the equality holds if and only if $\rho_+ = \rho_-$ (see [40, Page 177, Theorem 7.8]). Thus, we may denote the common orbital function as $\phi = \psi_+ = \psi_-$, which minimizes the functional

$$\mathscr{E}_0(\phi) = \int |\nabla\phi|^2\,\mathrm{d}x + 2\int V(x)|\phi|^2\,\mathrm{d}x + 2\iint \frac{|\phi(x)|^2|\phi(y)|^2}{|x-y|}\,\mathrm{d}x\,\mathrm{d}y. \tag{13}$$

Note that this functional has the same form as the restricted Hartree model treated in [43, Theorem II.2], which guarantees the existence of a minimizer. Moreover, the minimizer is non-negative without loss of generality and satisfies the Euler-Lagrange equation

$$-\frac{1}{2}\Delta\phi + E_0\phi + V\phi + 2(v_c * |\phi|^2)\phi = 0 \tag{14}$$

where $v_c(x) = |x|^{-1}$ denotes the Coulomb kernel and $E_0 \geq 0$ is the Lagrangian multiplier. We now show that E_0 must be strictly positive. Suppose $E_0 = 0$, define $W := V + 2v_c * |\phi|^2$, we have

$$-\frac{1}{2}\Delta\phi + W\phi = 0. \tag{15}$$

Using Newton's theorem, the spherical average of W, denoted by $\overline{W}$ is non-positive outside the ball B_R (since the ball contains all the nuclei charge). Thus, we get trivially that the positive part of $\overline{W}_+ =$

4

$\max\{\overline{W}, 0\} \in L^{3/2}(B_R^c)$. This implies that $\phi \notin L^2(B_R^c)$ by [41, Lemma 7.18], which is clearly a contradiction, since $\int |\phi|^2 = 1$. Therefore, $E_0 > 0$. This implies that the nuclear potential is properly binding in a similar sense to that explored in [55].

For a purpose that will be clear later, we also consider the variational problem (13) with more general mass constraints and denote the minimum as I_M:

$$
\begin{aligned}
I_M &:= \inf\left\{ \mathscr{E}_0(\phi) \mid \int |\phi|^2 = M/2 \right\} \\
&= \inf\left\{ \mathscr{E}_0(\phi) \mid \int |\phi|^2 \leq M/2 \right\} \\
&= \inf\left\{ \mathscr{E}_0(\sqrt{\rho}/\sqrt{2}) \mid \int \rho \leq M \right\},
\end{aligned}
\tag{16}
$$

where the second equality follows from the fact that I_M is monotonically decreasing as we can always put some excessive charge far away from the nuclei with negligible contribution to the energy. Furthermore, I_M is strictly convex for $M \in [0, M_c)$ for some $M_c \geq 2$, which follows the standard convexity argument applies to $\mathscr{E}_0(\sqrt{\rho}/\sqrt{2})$ as in the proof of parts (iii) and (iv) of [43, Corollary II.1] (see also the proof of convexity of the energy of the related Thomas-Fermi-von Weizsäcker theory in [8]). We also have the relation

$$
\left. \frac{\partial I_M}{\partial M} \right|_{M=2} = -E_0 < 0,
\tag{17}
$$

since E_0 is the Lagrange multiplier corresponding to the constraint $\int |\phi|^2 = M$. This in turn guarantees that $M_c > Z$, as in Part (i) of [43, Corollary II.1]. Therefore, denote $E_0(M)$ the corresponding Lagrange multiplier for I_M, we arrive at

$$
-\left. \frac{\partial E_0(M)}{\partial M} \right|_{M=2} = \left. \frac{\partial^2 I_M}{\partial M^2} \right|_{M=2} > 0.
\tag{18}
$$

Following the analysis of [42, Theorem 3.1] using elliptic estimates, one observes that if $\phi \in H^1$ a solution to (14), then $\phi \in H^2$.

2.2 Implicit function theorem analysis for small α

We consider (3) for α small. First of all, by restricting to the class of solutions symmetric with respect to reflection in x, we know there exists a delocalized solution obeying the correct symmetry properties. For $\alpha = 0$, (3) is a convex functional and there exists a *unique* delocalized solution $\phi = \psi_+ = \psi_-$ such that $\|\phi\|_{L^2} = 1$. The following result extends the uniqueness to small α.

Proposition 2.1. *For $0 \leq \alpha \leq \alpha_0$ sufficiently small, there exists a unique, delocalized minimizer to* (3) *with* $\|\phi\|_{L^2} = 1$. *The dependence upon α is C^1.*

The remainder of this section is devoted to the proof of Proposition 2.1. The idea is to construct a symmetric solution branch stemming from the unique solution at $\alpha = 0$ that comes from the convexity of the energy functional in that limit. While the positive α perturbation is non-convex, the Euler-Lagrange equations can be solved using a Lyapunov-Schmidt reduction. In fact, we will see that we can construct an implicit function theorem argument using the convexity at $\alpha = 0$ and in doing so, that locally only the symmetric branch will be possible. First, we will allow the branch to vary with respect to mass, then we will fix the Lagrange multipliers E_+ and E_- (in most cases we will observe $E_+ = E_-$ as a function of α to guarantee the mass 1 electron branch.

The Euler-Lagrange equations for $\mathscr{E}_{LDA,\alpha}$ give us a function on $(H^2)^2 \times \mathbb{R}^2$ defined as

$$
F(\psi_+, \psi_-; \alpha, E) = \begin{pmatrix} -\frac{1}{2}\Delta\psi_+ + E_+\psi_+ + V\psi_+ + \left(v_c * \left(|\psi_+|^2 + |\psi_-|^2\right)\right)\psi_+ - \frac{4}{3}\alpha|\psi_+|^{\frac{2}{3}}\psi_+ \\ -\frac{1}{2}\Delta\psi_- + E_-\psi_- + V\psi_- + \left(v_c * \left(|\psi_+|^2 + |\psi_-|^2\right)\right)\psi_- - \frac{4}{3}\alpha|\psi_-|^{\frac{2}{3}}\psi_- \end{pmatrix} = 0.
\tag{19}
$$

To apply the Lyapunov-Schmidt reduction, we need to address the kernel of the Jacobian with respect to $\psi_\pm$ for the Euler-Lagrange equations. This is given by the operator

$$DF_\psi(\psi_+, \psi_-; \alpha, E_+, E_-)\begin{pmatrix} f_+ \\ f_- \end{pmatrix} = \begin{pmatrix} L_+ f_+ + 2\psi_+ v_c * (\psi_- \bar{f}_-) \\ 2\psi_- v_c * (\psi_+ \bar{f}_+) + L_- f_- \end{pmatrix} \tag{20}$$

for

$$L_+(\psi_\pm; \alpha, E_+) f_+ = \left(-\frac{1}{2}\Delta + E_+ + V + v_c * \left(|\psi_+|^2 + |\psi_-|^2\right) - \frac{20}{9}\alpha|\psi_+|^{\frac{2}{3}}\right) f_+ + 2\psi_+ v_c * (\psi_+ \bar{f}_+)$$

and similarly

$$L_-(\psi_\pm; \alpha, E_-) f_- = \left(-\frac{1}{2}\Delta + E_- + V + v_c * \left(|\psi_+|^2 + |\psi_-|^2\right) - \frac{20}{9}\alpha|\psi_-|^{\frac{2}{3}}\right) f_- + 2\psi_- v_c * (\psi_- \bar{f}_-).$$

For $\phi = \psi_+ = \psi_-$, the unique solution at $\alpha = 0$ with resulting Lagrange multiplier E_0 stemming from the convexity of $E_{LDA,0}$, we have

$$DF_\psi(\phi, \phi; 0, E_0, E_0)\begin{pmatrix} f_+ \\ f_- \end{pmatrix} = \begin{pmatrix} L_{\phi,E_0} f_+ + 2\phi v_c * (\phi \bar{f}_-) \\ 2\phi v_c * (\phi \bar{f}_+) + L_{\phi,E_0} f_- \end{pmatrix}$$

for

$$L_{\phi,E_0} f = \left(-\frac{1}{2}\Delta + E_0 + V + 2v_c * |\phi|^2\right) f + 2\phi v_c * (\phi \bar{f}).$$

In the class of symmetric solutions, we actually have a reduced set of equations and can instead solve a scalar problem with parameters.

2.3   Analysis of the Linearized Operators for $\alpha = 0$

We prove here that at $\alpha = 0$, $\psi_+ = \psi_- = \phi$, $E = E_0$, then the linearized operator has a kernel, but it can only lead to solutions where ψ_+ and ψ_- take on different masses. This is a key step in applying the implicit function theorem in α locally. To see this, we linearize (14) to get the operator

$$\widetilde{L}_{\phi,E_0} f = \left(-\frac{1}{2}\Delta + E_0 + V + 2v_c * |\phi|^2\right) f + 4\phi v_c * (\phi \bar{f}). \tag{21}$$

We observe that the operator $\widetilde{L}_{\phi,E_0}$ can be written in the form

$$\widetilde{L}_{\phi,E_0} = -\frac{1}{2}\Delta + E_0 + V + V_\phi + W_\phi,$$

where

$$V_\phi f = E_0 f + V f + 2v_c * |\phi|^2 f$$

is a self-adjoint local operator with $1/|x|$ decay and

$$W_\phi = 4\phi v_c * (\phi \bar{f})$$

is a self-adjoint non-local operator with exponential decay. In both cases, we will see that these are bounded, relatively compact perturbations of the Laplacian, and hence argue that the continuous spectrum of L_{ϕ,E_0} is on the set $[E_0, \infty)$. Then, we will use a linear argument based around the convexity of solutions to the problem at $\alpha = 0$ to show that the kernel of L_{ϕ,E_0} is trivial. This will allow us to construct a family of solutions using the implicit function theorem.

Since $V + V_\phi + W_\phi$ is a relatively compact perturbation, we observe that the continuous spectrum of L_{ϕ,E_0} is the interval $[E_0, \infty)$ by applying Weyl's Theorem, see [51, 40] for instance, or [39] where the functional analysis of Hartree-style equations is discussed in some detail.

Lemma 2.2. *The operator $\widetilde{L}_{\phi, E_0}$ has only trivial kernel.*

Proof. Let us assume to the contrary there exists $f \in H^2$ such that

$$\widetilde{L}_{\phi, E_0} f = 0.$$

Then, we observe that

$$0 = \left\langle (-\tfrac{1}{2}\Delta + E_0 + V + V_\phi)f, f \right\rangle + \left\langle W_\phi f, f \right\rangle.$$

However, given the structure of W_ρ, it turns out that

$$\langle W_\phi f, f \rangle > 0 \text{ for } f \neq 0.$$

This is easiest to see this is by looking at the inner product in Fourier space.

Taking the orthogonal decomposition $f = \alpha\phi + \phi^\perp$ and using that ϕ is the unique kernel of the operator $L_- = -\tfrac{1}{2}\Delta + E_0 + V + V_\phi$ and hence if $\phi^\perp \neq 0$, we observe that we have a contradiction immediately from the coercivity of L_-. However, if $\phi^\perp = 0$, then $\alpha \neq 0$ and we still observe positivity from the term $\langle W_\phi f, f \rangle$.

$\square$

Remark 2.1. This is a similar strategy to that of standard semi-linear problems, however in such a case the perturbation of the L_- operator is negative in total and hence the spectral theory of the linearized operator must be understood in much greater detail. Here, the perturbation is actually positive, so the arguments are greatly simplified. It is also essential that we have a potential here, which has broken the translation invariance.

2.4 Construction of solutions near $\alpha = 0$

Claim 2.3. *Since $E_{LDA,0}$ is a convex functional, the Jacobian $DF_\psi(\phi, \phi; 0, E_0)$ has kernel given by $\mathrm{span}\{(\phi, -\phi)\}$ and as a result, a unique C^1 path in (α, E) can be constructed through symmetric functions in $H^2 \times H^2$ using the implicit function theorem with fixed constraint $\|\psi_\pm\|_{L^2} = 1$.*

Proof. We must study the invertibility of DF at $\alpha = 0$. In the restricted space, $\psi_+ = \psi_-$, the invertibility is established in Lemma 2.2 through the invertibility of $\widetilde{L}$. The remainder of the argument follows from a fairly standard application of the implicit function theorem. Indeed, we observe that if $DF\vec{f} = 0$, then $\widetilde{L}(f_1 + f_2) = 0$ for $\vec{f} = (f_1, f_2)$. Hence, either $f_1 + f_2$ is a non-trivial kernel function of $\widetilde{L}$ or $f = f_1 = -f_2$ and f_1 is a non-trivial kernel function for a modified operator

$$\mathscr{L}_{\phi, E_0} f = \left(-\frac{1}{2}\Delta + E_0 + V + 2v_c * |\phi|^2 \right) f,$$

which through the equation satisfies $\mathscr{L}\phi = 0$. Since $\phi > 0$, it is the ground state and simple, which establishes the result on the spectrum.

We note that the nature of the kernel is not so surprising at $\alpha = 0$, as a major symmetry of $E_{LDA,0}$ would be to simply use a rotation of (ψ_+, ψ_-), which is an invariant of the Lagrangian. However, given that at $\alpha = 0$, we have $\psi_+ = \psi_- = \phi$, this symmetry generates no new solutions except the one we have found in the kernel. Using the convexity, we have uniqueness of the symmetric solution ϕ as a minimizer having fixed mass $\|\phi\|_{L^2}^2 = 1$.

The remaining proof relies on varying E using the standard Lyapunov-Schmidt construction of $\phi(E, \alpha)$ solving the Euler-Lagrange equation,

$$(\psi_+, \psi_-) = (\phi, \phi) + c_0(\phi, -\phi) + (\eta_+, -\eta_-),$$

7

for $\alpha \sim c_0^2$, $\int (\eta_+ + \eta_-) \phi \, dx = 0$ and $\|\eta\| \sim c_0^2$, see [37, Proposition 1] for a general discussion of the method. We observe that

$$\|\eta(c_0, E_\pm - E_0, \alpha)\|_{H^2} \lesssim c_0^2, \quad |E_\pm - E_0| \lesssim c_0^2.$$

Indeed, expanding about (ϕ, ϕ) in this fashion we have

$$F(\phi, \phi; 0, E_0) + DF(\phi, \phi; 0, E_\pm)\begin{pmatrix} \eta_+ \\ \eta_- \end{pmatrix} + \mathcal{O}\left(|\eta|^2 + c_0^2 + \alpha + (E_\pm - E_0)\phi\right) = \begin{pmatrix} 0 \\ 0 \end{pmatrix}. \tag{22}$$

We note here that the linearization is $DF(\phi, \phi; 0, E_\pm)$ and not $DF(\phi, \phi; 0, E_0)$. Using the properties of DF, ϕ and E_0, we then observe that we can first solve for $(\eta_+, \eta_-) = (\eta_+, \eta_-)(c_0, E_\pm, \alpha)$ in

$$\begin{pmatrix} \eta_+ \\ \eta_- \end{pmatrix} = (P^\perp DF(\phi, \phi; 0, E_\pm) P^\perp)^{-1} P^\perp \mathcal{O}\left(|\eta|^2 + c_0^2 + \alpha + (E_\pm - E_0)\phi\right) \tag{23}$$

with $P^\perp \vec{f} = \vec{f} - \langle \vec{f}, (\phi, -\phi)^\mathrm{T} \rangle (\phi, -\phi)^\mathrm{T}$ applying the standard Implicit Function Theorem. This implies that (22) is given by

$$\begin{aligned}
\left(-\frac{1}{2}\Delta + E_\pm + V\right)\eta_\pm &= (E_\pm - E_0)\phi + c_0(E_\pm - E_0)\phi - \alpha|\phi(1 \pm c_0) + \eta_\pm|^{\frac{2}{3}}(\phi(1 \pm c_0) + \eta_\pm) \\
&\quad + v_c * \left[2c_0^2\phi^2 + 2(1 + c_0)\phi\eta_+ + 2(1 - c_0)\phi\eta_- + \eta_+^2 + \eta_-^2\right]\phi \\
&\quad \pm c_0 v_c * \left[2c_0^2\phi^2 + 2(1 + c_0)\phi\eta_+ + 2(1 - c_0)\phi\eta_- + \eta_+^2 + \eta_-^2\right]\phi \\
&\quad + v_c * \left[2\phi^2 + 2c_0^2\phi^2 + 2(1 + c_0)\phi\eta_+ + 2(1 - c_0)\phi\eta_- + \eta_+^2 + \eta_-^2\right]\eta_\pm.
\end{aligned}$$

As we are taking $|E_\pm - E_0|$ small, $P^\perp DF(\phi, \phi; 0, E_\pm) P^\perp$ is invertible since $P^\perp DF(\phi, \phi; 0, E_0) P^\perp$ is invertible. We observe that by the Implicit Function Theorem we have

$$\|\vec{\eta}\|_{H^2} \le C\left(c_0^2 + \alpha + (E_+ - E_0) + (E_- - E_0)\right).$$

Projecting (22) onto $(\phi, -\phi)$, we have[1]

$$(E_+ - E_0) - (E_- - E_0) + c_0[(E_+ - E_0) + (E_- - E_0)] + \mathcal{O}\left(\|\vec{\eta}\|_{L^2}^2 + c_0^3 + \alpha\left(c_0 + \|\vec{\eta}\|_{L^2}^{\frac{2}{3}}\right)\right) = 0,$$

which allows us to use the Implicit Function Theorem once again to solve for E_+ given E_- and write for instance

$$(E_+ - E_0) = (E_+ - E_0)(c_0, \alpha, E_- - E_0),$$

with

$$|E_+ - E_0| \le C\left(c_0^3 + \alpha c_0 + \alpha^{\frac{5}{3}} + |E_- - E_0|\right).$$

Now, using the two constraint equations for the mass, we have

$$\int (2c_0\phi + c_0^2\phi^2 + 2(1 + c_0)\phi\eta_+ + \eta_+^2)\, dx = 0 \tag{25}$$

and

$$\int (-2c_0\phi + c_0^2\phi^2 + 2(1 - c_0)\phi\eta_- + \eta_-^2)\, dx = 0. \tag{26}$$

---

[1] Here, we use the following bound pointed out to the authors by N. Visciglia: Let $\alpha > 0$ be given. Then for every $a, b \in \mathbb{C}$ we have the following inequality:

$$\left|(a + b)|a + b|^\alpha - a|a|^\alpha - b|b|^\alpha\right| \lesssim (|a||b|^\alpha + |b||a|^\alpha). \tag{24}$$

Using the linear combination (25) + (26) and the orthogonality of (η_+, η_-) to $(\phi, -\phi)$, we first observe that

$$|E_- - E_0| \leq C(\alpha + c_0^2),$$

which implies for the linear combination (25) − (26), we can observe that

$$c_0^2 \leq C\alpha.$$

Once the overall dependence upon α has been determined, we realize that on the branch described above in (25) and (26), everything is indeed lower order to the $\mathcal{O}(c_0)$ term. Thus, $c_0 = 0$ lest we not move off the mass 1 branch.

Remark 2.2. From the sign changes (25) and (26), we expect that with no mass constraint the branch construction stemming from the kernel of DF to leading order leads to $E_+ = -E_-$. If we were allowed to make such a symmetric reduction, the arguments above can be simplified.

2.5 Construction of the local branch under the symmetry assumption

Using that the linearization preserves symmetric solutions, let us limit ourselves to solutions of the simplified Euler-Lagrange equation for $\phi(E, \alpha)$ given by

$$-\frac{1}{2}\Delta\phi + E\phi - V\phi + 2\int \frac{|\phi|^2(y)}{|x-y|}\,dy\,\phi - \alpha|\phi|^{\frac{2}{3}}\phi = 0.$$

The mass of ϕ is

$$M(E, \alpha) = \int |\phi|^2 dx.$$

By construction, $M(E_0, 0) = 1$. To find mass 1 states, using that $\phi = \phi(E, \alpha)$, we wish to find $E(\alpha)$ solving

$$M(E, \alpha) := \int |\phi(E(\alpha), \alpha)|^2 dx - 1 = 0.$$

Hence, we wish to apply the Implicit Function Theorem once more, which guarantees the solvability of $E(\alpha)$ provided

$$\frac{\partial M}{\partial E}\Big|_{E=E_0, \alpha=0} \neq 0.$$

However, at $\alpha = 0$ this follows directly from (18). Using the Implicit Function Theorem for a small range of α, there is an $E = E(\alpha)$ satisfying the mass equation.

$\qquad\qquad\qquad\qquad\qquad\qquad\qquad\qquad\qquad\qquad\qquad\qquad\qquad\qquad\qquad\qquad\qquad\qquad\quad \square$

3 Localization and symmetry breaking for large α

3.1 A priori energy estimate

We consider a variational problem with only the kinetic and exchange terms:

$$\min_{\varphi:\int|\varphi|^2=1} F(\varphi) = \frac{1}{2}\int |\nabla\varphi|^2 - \int |\varphi|^{8/3}. \tag{27}$$

It is now classical in the theory of nonlinear Schrödinger equations that the minimizer of (27) exists and is radial and unique up to a translation, see for instance [57]. Denote φ the minimizer of (27) centered at zero, it satisfies

$$-\frac{1}{2}\Delta\varphi - \frac{4}{3}|\varphi|^{2/3}\varphi + E\varphi = 0 \tag{28}$$

9

with E being a strictly positive Lagrange multiplier. Moreover, φ decays exponentially as $|x| \to \infty$.

We consider dilation operators $\{D_t\}$ that preserve the L^2 norm

$$(D_t f)(x) = t^{3/2} f(tx). \tag{29}$$

Let x_+ and x_- minimize

$$\min\left(\left\|\nabla\psi_\pm - \nabla(D_\alpha\varphi)(\cdot - x_\pm)\right\|_{L^2}^2 + E\left\|\psi_\pm - (D_\alpha\varphi)(\cdot - x_\pm)\right\|_{L^2}^2\right). \tag{30}$$

We write the remainder as

$$\psi_\pm = \left(D_\alpha(\varphi + w_\pm)\right)(\cdot - x_\pm). \tag{31}$$

Correspondingly, we have $\varphi = D_\alpha^{-1}\tau_{x_\pm}^{-1}(\psi_\pm) - w_\pm$, to simplify notation, we denote

$$\widetilde{\psi}_\pm = D_\alpha^{-1}\tau_{x_\pm}^{-1}\psi_\pm = \alpha^{-3/2}\psi_\pm\left(\frac{x + x_\pm}{\alpha}\right). \tag{32}$$

As $\{\psi_\pm\}$ minimize E_α, we have

$$0 \le E_\alpha\left((D_\alpha\varphi)(\cdot - x_+), (D_\alpha\varphi)(\cdot - x_-)\right) - E_\alpha(\psi_+, \psi_-)$$
$$= \alpha^2\left(2F(\varphi) - F(\widetilde{\psi}_+) - F(\widetilde{\psi}_-)\right) + \int V(\rho_\varphi - \rho_\psi) \tag{33}$$
$$+ \frac{1}{2}\iint \frac{\rho_\varphi(x)\rho_\varphi(y)}{|x-y|}\,\mathrm{d}x\,\mathrm{d}y - \frac{1}{2}\iint \frac{\rho_\psi(x)\rho_\psi(y)}{|x-y|}\,\mathrm{d}x\,\mathrm{d}y,$$

where

$$\rho_\varphi(x) = \left|(D_\alpha\varphi)(x - x_+)\right|^2 + \left|(D_\alpha\varphi)(x - x_-)\right|^2.$$

Note that $\frac{1}{2}\iint \frac{\rho_\psi(x)\rho_\psi(y)}{|x-y|}\,\mathrm{d}x\,\mathrm{d}y \ge 0$, rearranging the terms, we obtain

$$F(\widetilde{\psi}_+) + F(\widetilde{\psi}_-) - 2F(\varphi) \le \frac{1}{\alpha^2}\left(\int V\rho_\varphi + \frac{1}{2}\iint \frac{\rho_\varphi(x)\rho_\varphi(y)}{|x-y|}\,\mathrm{d}x\,\mathrm{d}y\right) - \frac{1}{\alpha^2}\int V\rho_\psi\,\mathrm{d}x. \tag{34}$$

By the scaling of $D_\alpha\varphi$, we have

$$\int V\rho_\varphi + \frac{1}{2}\iint \frac{\rho_\varphi(x)\rho_\varphi(y)}{|x-y|}\,\mathrm{d}x\,\mathrm{d}y \le C\alpha. \tag{35}$$

To control the last term on the right hand side, recall that by Hardy's uncertainty principle, we have for any $X \in \mathbb{R}^3$ and $f \in H^1$

$$\int \frac{1}{|x-X|}|f(x)|^2\,\mathrm{d}x \le 4\|f\|\,\|\nabla f\|. \tag{36}$$

Therefore, since $\|\psi_\pm\| = 1$, we have

$$-\int V\rho_\psi\,\mathrm{d}x = \int \frac{1}{|x-e_1|}\left(|\psi_+|^2 + |\psi_-|^2\right)\mathrm{d}x + \int \frac{1}{|x+e_1|}\left(|\psi_+|^2 + |\psi_-|^2\right)\mathrm{d}x \le C\left(\|\nabla\psi_-\| + \|\nabla\psi_+\|\right). \tag{37}$$

Thus, we arrive at

$$\begin{aligned}
F(\widetilde{\psi}_+) + F(\widetilde{\psi}_-) - 2F(\varphi) &\le \frac{C}{\alpha} + \frac{C}{\alpha^2}\left(\|\nabla\psi_+\| + \|\nabla\psi_-\|\right) \\
&\le \frac{C}{\alpha} + \frac{C}{\alpha^2}\left(\|\nabla D_\alpha(\varphi + w_+)\| + \|\nabla D_\alpha(\varphi + w_-)\|\right) \\
&\le \frac{C}{\alpha} + \frac{C}{\alpha}\left(\|\nabla w_+\| + \|\nabla w_-\|\right) \\
&\le \frac{C}{\alpha} + \frac{C}{\alpha}\left(\|\nabla w_+\|^2 + \|\nabla w_-\|^2\right).
\end{aligned} \tag{38}$$

Using the result in [62] for the semilinear functional (27), the left hand side of (38) is bounded from below as

$$F(\widetilde{\psi}_+) + F(\widetilde{\psi}_-) - 2F(\varphi) \geq g(\|w_+\|_{H^1}) + g(\|w_-\|_{H^1}), \tag{39}$$

where

$$g(t) = ct^2(1 - at^\theta - bt^4) \quad \text{with} \quad a, b, c, \theta > 0. \tag{40}$$

Combining (38) and (39), we conclude that

$$\lim_{\alpha \to \infty} \|w_\pm\|_{H^1} = \lim_{\alpha \to \infty} \|\widetilde{\psi}_\pm - \varphi\|_{H^1} = 0. \tag{41}$$

In other words, up to translation and dilation, the minimizer of (7) is close to the minimizer of the semilinear problem (27) for α large.

3.2 Location optimization

We further determine the translation vectors $x_\pm$. We claim that as $\alpha \to \infty$, the translation vectors $x_\pm \to \pm e_1$ (up to swapping x_+ and x_-, recall that swapping ψ_+ and ψ_- does not change the energy). The key observation is that the kinetic and exchange energy terms are invariant with respect to translation, and hence $x_\pm$ are determined by the potential and Coulomb repulsion terms, which are higher order terms when α is large.

For this, we consider shifted minimizers

$$\widehat{\psi}_+ = \psi_+(\cdot + e_1 + x_+) \quad \text{and} \quad \widehat{\psi}_- = \psi_-(\cdot - e_1 + x_-). \tag{42}$$

By (31), we have

$$\widehat{\psi}_\pm = (D_\alpha \varphi)(\cdot \pm e_1) + (D_\alpha w_\pm)(\cdot \pm e_1). \tag{43}$$

Due to minimality, we have

$$
\begin{aligned}
0 &\leq E_\alpha(\widehat{\psi}_+, \widehat{\psi}_-) - E_\alpha(\psi_+, \psi_-) \\
&= \int V(\rho_{\widehat{\psi}} - \rho_\psi) + \frac{1}{2} \iint \frac{\rho_{\widehat{\psi}}(x)\rho_{\widehat{\psi}}(y)}{|x-y|} \,dx\,dy - \frac{1}{2} \iint \frac{\rho_\psi(x)\rho_\psi(y)}{|x-y|} \,dx\,dy.
\end{aligned}
\tag{44}
$$

Recall ρ_φ and similarly define $\rho_{\widehat{\varphi}}$ as

$$
\begin{aligned}
\rho_\varphi(x) &= |(D_\alpha \varphi)(x - x_+)|^2 + |(D_\alpha \varphi)(x - x_-)|^2; \\
\rho_{\widehat{\varphi}}(x) &= |(D_\alpha \varphi)(x + e_1)|^2 + |(D_\alpha \varphi)(x - e_1)|^2.
\end{aligned}
$$

Denoting

$$\delta_{\mathrm{VC}}(\rho_1, \rho_2) = \int V(\rho_1 - \rho_2) + \frac{1}{2} \iint \frac{\rho_1(x)\rho_1(y)}{|x-y|} \,dx\,dy - \frac{1}{2} \iint \frac{\rho_2(x)\rho_2(y)}{|x-y|} \,dx\,dy, \tag{45}$$

we rewrite (44) as

$$\delta_{\mathrm{VC}}(\rho_{\widehat{\psi}}, \rho_\psi) = \delta_{\mathrm{VC}}(\rho_{\widehat{\psi}}, \rho_{\widehat{\varphi}}) + \delta_{\mathrm{VC}}(\rho_{\widehat{\varphi}}, \rho_\varphi) + \delta_{\mathrm{VC}}(\rho_\varphi, \rho_\psi) \geq 0. \tag{46}$$

Let us estimate $\delta_{\mathrm{VC}}(\rho_\varphi, \rho_\psi)$ first. For the potential term, using (36) for $f = |\rho_\varphi - \rho_\psi|^{1/2}$,

$$\int |V(\rho_\varphi - \rho_\psi)| \leq C \left\||\rho_\varphi - \rho_\psi|^{1/2}\right\|_{L^2} \left\|\nabla |\rho_\varphi - \rho_\psi|^{1/2}\right\|_{L^2} \leq C \left\|\nabla |\rho_\varphi - \rho_\psi|^{1/2}\right\|_{L^2}. \tag{47}$$

For the difference in Coulomb energy

$$\left| \frac{1}{2} \iint \frac{\rho_\varphi(x)\rho_\varphi(y)}{|x-y|} \,\mathrm{d}x\,\mathrm{d}y - \frac{1}{2} \iint \frac{\rho_\psi(x)\rho_\psi(y)}{|x-y|} \,\mathrm{d}x\,\mathrm{d}y \right|$$

$$\le \iint \frac{\left|\rho_\varphi - \rho_\psi\right|(x)\rho_\varphi(y)}{|x-y|} \,\mathrm{d}x\,\mathrm{d}y + \frac{1}{2} \iint \frac{(\rho_\varphi - \rho_\psi)(x)(\rho_\varphi - \rho_\psi)(y)}{|x-y|} \,\mathrm{d}x\,\mathrm{d}y$$

$$\le C \left\| \rho_\varphi - \rho_\psi \right\|_{L^{3/2}} \left\| \rho_\varphi \right\|_{L^1} + C \left\| \rho_\varphi - \rho_\psi \right\|_{L^{6/5}}^2, \quad (48)$$

where the last line uses the Hardy-Littlewood-Sobolev inequality. Observe that using interpolation and Gargliardo-Nirenberg-Sobolev inequality, we have

$$\left\| f \right\|_{L^{6/5}} \le \left\| f \right\|_{L^1}^{3/4} \left\| f \right\|_{L^3}^{1/4} \le C \left\| f \right\|_{L^1}^{3/4} \left\| \nabla\sqrt{f} \right\|_{L^2}^{1/2}, \quad (49)$$

$$\left\| f \right\|_{L^{3/2}} \le \left\| f \right\|_{L^1}^{1/2} \left\| f \right\|_{L^3}^{1/2} \le C \left\| f \right\|_{L^1}^{1/2} \left\| \nabla\sqrt{f} \right\|_{L^2}. \quad (50)$$

Combined with the above three inequalities, we get

$$\left| \frac{1}{2} \iint \frac{\rho_\varphi(x)\rho_\varphi(y)}{|x-y|} \,\mathrm{d}x\,\mathrm{d}y - \frac{1}{2} \iint \frac{\rho_\psi(x)\rho_\psi(y)}{|x-y|} \,\mathrm{d}x\,\mathrm{d}y \right| \le C \left\| \nabla\left|\rho_\varphi - \rho_\psi\right|^{1/2} \right\|_{L^2}. \quad (51)$$

To estimate the right hand side of (47) and (51), by definition

$$\left\| \nabla\left|\rho_\varphi - \rho_\psi\right|^{1/2} \right\|_{L^2} \le \left\| \nabla\left(2\left|D_\alpha\varphi\right|\left|D_\alpha w_+\right| + 2\left|D_\alpha\varphi\right|\left|D_\alpha w_-\right| + \left|D_\alpha w_+\right|^2 + \left|D_\alpha w_-\right|^2\right)^{1/2} \right\|_{L^2}$$

$$\le C \left(\left\| \nabla\left(\left|D_\alpha\varphi\right|\left|D_\alpha w_+\right|\right)^{1/2} \right\|_{L^2} + \left\| \nabla\left(\left|D_\alpha\varphi\right|\left|D_\alpha w_-\right|\right)^{1/2} \right\|_{L^2} \right.$$

$$\left. + \left\| \nabla\left|D_\alpha w_+\right| \right\|_{L^2} + \left\| \nabla\left|D_\alpha w_-\right| \right\|_{L^2} \right) \quad (52)$$

$$\le C\alpha\left(\left\| w_+ \right\|_{H^1} + \left\| w_- \right\|_{H^1} \right),$$

where we have used the convexity of $\left|\nabla\sqrt{\rho}\right|^2$ and the Cauchy-Schwartz inequality. Note that the α prefactor on the right hand side is natural from the scaling, since the characteristic length scale of ρ_φ is order $1/\alpha$ due to the construction by dilation. Therefore, to sum up,

$$\left| \delta_{\mathrm{VC}}(\rho_\varphi, \rho_\psi) \right| \le C\alpha\left(\left\| w_+ \right\|_{H^1} + \left\| w_- \right\|_{H^1} \right). \quad (53)$$

It is easy to check that the same upper bound also holds for $\delta_{\mathrm{VC}}(\rho_{\widehat{\varphi}}, \rho_{\widehat{\psi}})$. Thus,

$$\delta_{\mathrm{VC}}(\rho_{\widehat{\varphi}}, \rho_\varphi) \ge -C\alpha\left(\left\| w_+ \right\|_{H^1} + \left\| w_- \right\|_{H^1} \right). \quad (54)$$

We now turn the above estimate of the Coulomb energy difference into an estimate of the translation vectors $x_\pm$. For this, we calculate more explicitly $\delta_{\mathrm{VC}}(\rho_{\widehat{\varphi}}, \rho_\varphi)$ (recall that φ is the unique radial minimizer to the semilinear functional (27)). We have

$$\delta_{\mathrm{VC}}(\rho_\varphi, \rho_{\widehat{\varphi}}) = \int V(\rho_\varphi - \rho_{\widehat{\varphi}}) + \iint \frac{\left|D_\alpha\varphi\right|^2(x-x_+)\left|D_\alpha\varphi\right|^2(y-x_-)}{|x-y|} \,\mathrm{d}x\,\mathrm{d}y$$

$$- \iint \frac{\left|D_\alpha\varphi\right|^2(x-x_+)\left|D_\alpha\varphi\right|^2(y-x_-)}{|x-y|} \,\mathrm{d}x\,\mathrm{d}y. \quad (55)$$

As φ decays exponentially, we have

$$\iint \frac{|D_\alpha \varphi|^2 (x - x_+) |D_\alpha \varphi|^2 (y - x_-)}{|x - y|} \, dx \, dy \lesssim \frac{1}{\alpha}, \tag{56}$$

and therefore

$$\int V(\rho_\varphi - \rho_{\widehat{\varphi}}) + \iint \frac{|D_\alpha \varphi|^2 (x - x_+) |D_\alpha \varphi|^2 (y - x_-)}{|x - y|} \, dx \, dy \le C\alpha \big(\|w_+\|_{H^1} + \|w_-\|_{H^1} \big) + \mathcal{O}(\alpha^{-1}). \tag{57}$$

This implies

$$\lim_{\alpha \to \infty} \frac{1}{\alpha} \int V(\rho_\varphi - \rho_{\widehat{\varphi}})$$

$$= \lim_{\alpha \to \infty} -\frac{1}{\alpha} \int \left(\frac{1}{|x - e_1|} + \frac{1}{|x + e_1|} \right) \big(|D_\alpha \varphi|^2 (x - x_+) - |D_\alpha \varphi|^2 (x - e_1) \big) \, dx$$

$$+ \lim_{\alpha \to \infty} -\frac{1}{\alpha} \int \left(\frac{1}{|x - e_1|} + \frac{1}{|x + e_1|} \right) \big(|D_\alpha \varphi|^2 (x - x_-) - |D_\alpha \varphi|^2 (x + e_1) \big) \, dx = 0, \tag{58}$$

since the second term on the left hand side of (57) is non-negative. Note that the two limits in the middle of the above equation are both non-negative. We have

$$\lim_{\alpha \to \infty} -\frac{1}{\alpha} \int \left(\frac{1}{|x - e_1|} + \frac{1}{|x + e_1|} \right) \big(|D_\alpha \varphi|^2 (x - x_+) - |D_\alpha \varphi|^2 (x - e_1) \big) \, dx = 0. \tag{59}$$

This implies that $\min\{|x_+ - e_1|, |x_+ + e_1|\}$ converges to zero, and similarly for x_-. Thus, as $\alpha \to \infty$, $x_\pm$ approaches $\{e_1, -e_1\}$. They cannot converge to the same point, as otherwise the Coulomb interaction is obviously higher. Therefore, we arrive at the conclusion.

4 Numerical solution to Kohn-Sham SDFT (KS-SDFT) equations for ψ_+ and ψ_- as a function of α

The variation of the energy functional given in Eq. (3) with normalization constraints, leads to Euler-Lagrange equations defining the spin up, ψ_+, and the spin down, ψ_-, KS-SDFT orbital solutions as a function of exchange strength α. In this section we outline the finite element methods (FEM) [9, 14] we used to produce numerical solutions to these equations and determine their stability. These solutions, characterized by the symmetry of the orbital functions and their localization within the molecular framework, were used to explore the transitions between the regions of stability identified by the theorems in Sections 2 and 3. In the process of generating these numerical solutions additional stable solution to the Euler Lagrange equations are identified and their stationary character validated via Hessian analysis (see appendix). These may have important consequences for the application of Kohn-Sham methods but were not analyzed above.

An important feature of the FEM approach we used is that the expansions of ψ_- and ψ_+ in the FEM basis [4] are not constrained by any preconceived notion as to the nature of the solution as is implicit in the atomic orbital expansion basis of quantum chemistry software [47, 58, 23]. This is particularly important in our application because of the forms of the KS solutions to Eq.(3) as a function of α (e.g. for large α) are unknown. The details of the numerical problem and the FEM method we developed for its solution are described in more detail in the Appendix. A novel feature of the numerical method we have used is that its time to solution scales linearly with the size of the basis [35].

4.1 Overview of numerical method (FEM)

Our numerical implementations are based on application of the Python FEniCS finite element (FEM) package [4] [35], which is a collection of free software with an extensive list of features for automated, efficient finite element solution methods for differential equations. The source codes implementing the linear scaling finite element solver described below can be found at `https://fenicsproject.org/`. More details specific to our calculation are given in the Appendix.

The FEM calculation domain used here is a fixed square box of dimension $50 \times 50 \times 50$ atomic units which easily contains the H_2 molecule (size ≈ 2 atomic units). Because the bound state molecular orbitals decay exponentially away from the positions of the nucleus, we apply zero boundary conditions at the domain edges for the wave functions. The Coulomb potentials are calculated from Poisson's equation using free space boundary conditions. The singularities of the attractive nuclear potentials, Eq. (1) are removed by adding a small positive constant in the denominator [35].

To accommodate the more rapid variation of the ψ functions near the atomic nucleus the finite element grid is adapted within the domain, see Figure 1. This is an essential feature of atomic and molecular electronic structure calculations [16, 38, 17] that do not introduce pseudopotentials [18].
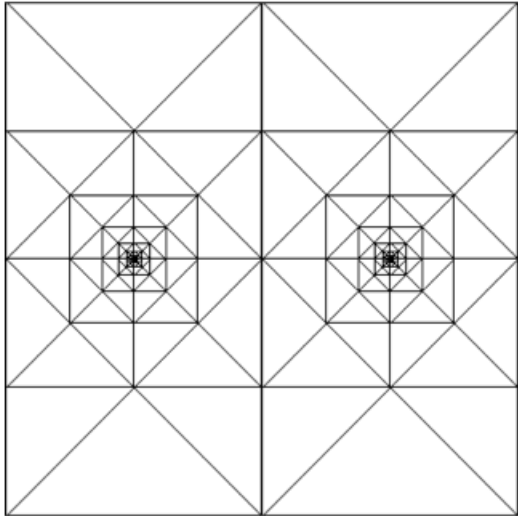

Figure 1: A representation of the finite element grid used in calculation. Each triangle represents a tetrahedron in the real calculation. Note that the density of the mesh is significantly increased near the two atomic nuclei (see appendix for further discussion as to how this mesh is generated).

In the FEM calculation each molecular orbital (ψ_+ or ψ_-) is written as an expansion in a finite element basis, η_i, with local support centered on the grid points in Figure 1[4], giving,

$$\psi_\pm = \sum_{i=1}^{M} c_{\pm,i} \eta_i. \tag{60}$$

There are M basis functions, where M is the total number of points in the grid and η_i the finite element basis functions (piecewise linear elements with local support) (see Appendix and [16] for more detail). The variation of the functional Eq. (3) expanded in the basis as in Eq. (60) leads to generalized eigenvalue

14

problems which must be solved self-consistently. These may be written as,

$$(-\frac{1}{2}\Delta - \epsilon_i)\psi_\pm = V(\rho)\psi_\pm. \tag{61}$$

where total electron density is $\rho = (\psi_-^2 + \psi_+^2)$. The eigenvalue problem is solved using an iterative process in which for step k the $\psi_\pm$ on right hand side of Eq. (61) and the orbital energies, $\epsilon_\pm^k$, at step k are assigned the the values and functionality from the $k-1$ step (see Appendix and [35]).

Eq. (61) is solved using the FEniCS software package (see Appendix and [35] for more detail). This package implements a conjugate gradient solver (generalized minimal residual method, GMRES [56]) after preconditioning with an algebraic multigrid preconditioner (AMG, BoomerAMG from the Hypre Library [2, 15, 61, 59, 27]). The application of the AMG solver leads to the linear in basis set time to solution feature of the numerical method.

An initial guess for the molecular orbitals (MOs) for the FEM solutions is necessary to start the iteration. Here we used H atom Slater Type Orbitals (STO-3G) generated from the NWChem data base [60] to form molecular orbitals for all α. Given two STO-3G functions centered on the atom center and designated as ϕ_1 and ϕ_2. The initial MOs for symmetric solution are $(\phi_1 + \phi_2)/2$ while the initial states when localized solutions are expected as ϕ_1 and ϕ_2 respectively, see [34, 23]. When α is very small, even the initial MOs are localized states ϕ_1 and ϕ_2, the final solution becomes delocalized state. For very large α the final solution may not be well approximated by this initial condition. However, we have not had problems with convergence of the method described in the appendix.

4.2 Numerical Results of DFT/ FEM calculations

The solution to the optimization problem posed by Eq. (3) are function of the internuclear distance, R, and the strength of the Dirac exchange, α. Consistent with the Pauli principle (requirement of Fermion wave function being antisymmetric) we assign individual electrons either to a spin up ψ_+ or spin down ψ_- spin eigenvector (the spin orbitals functions are products of a spacial function and a spin up or down eigenvector). With the further approximation of Dirac exchange and integration over the spin degrees of freedom this leads to the Kohn-Sham (KS) local spin density functional form expressed in Eq. (3)[48].

Formal results identifying features of the minimizers of Eq. (3) are given above. This is a two electron problem. In this formalism the forms of the spacial parts of the orbital wave functions are completely independent and the symmetry of the total density is not constrained. However, for most of the stationary solutions that we have found the total electron density has the symmetry of the H_2 molecule. We have shown this to be true for the lowest energy solution of Eq. (3) in both the large α and small α limits that we have proven to exist above. On the other hand, as we will illustrate in the following, the symmetry of the spacial parts of the individual spin orbitals may be broken in a way that still preserves the symmetry of the molecule for the total density. This break in symmetry occurs with a bifurcation and leads to electron localization. In applications of DFT to large molecules or condensed materials this localization is interpreted in term of the observed spin states of lattices (or molecules) (e.g. antiferromagnetic states in condensed materials [21, 26, 49]) . Thus the prediction of this spin ordering present in these states is an important objective of the application of DFT methods to molecular and condensed matter systems. The accuracies of the total energies are within 0.02 au for the H_2 molecule in our calculations.

4.2.1 Bifurcation in the R dimension

The optimized total energy as the H_2 molecular bond is lengthened for at fixed $\alpha = 0.93$ (from Eq. (3) and α similar to the value used in the application of SLDA to molecular and condensed matter problems)

is shown in Figure 2. Remarkably for given α and sufficiently small R the solutions for orbital wave functions ψ_+ and ψ_- converge to the same function even under full variation with no symmetry restriction. This is consistent with the fixed R, small α analysis in Section 2. This solution is the same as the so called *restricted solution* generated by enforcing double filling (spin up and spin down electrons states) of a single spacial orbital to form the two electron wave function. That is the *the restricted* DFT (RDFT) solution in which ψ_+ and ψ_- are the same function is the lowest energy solution to the optimization problem posed in Eq. (3) even when each orbital function is varied independently without constraint. Similar behavior is observed in the Hartree or Hartree-Fock model of electronic structure for the two electron system. These solutions are important because the restricted DFT solutions are widely used in quantum chemistry applications [58, 23] and it is important to be aware of their region of stability.

As the H_2 bond length is extended as illustrated in Figure 2 ($R > \approx 2.75$au) the solution bifurcates creating two two electron product (singlet determinant [58, 48]) solutions. In the lowest energy state (lower branch, green line) one symmetry broken electron orbital (say the spin up state) is localized around one site and the other orbital function state (spin down) is localized around the 2nd (see green density distribution bottom right Figure 2). The product wave function (total density) for this branch leads to a spin localized density distribution (*spin up and spin down electrons localized on different atomic sites with total spin zero*). This spin distribution is consistent with an antiferromagnetic state for the H_2 molecule. Since spin ordered condensed systems are common targets for DFT prediction, this is an important dimension for variation in designing DFT representations of spin ordered systems [21, 26, 49].

The upper energy branch in Figure 2 is a continuation of the restricted solution in which the spin up and spin down orbitals have the same spacial dependence (no localization, blue density distribution bottom right Figure 2). We note that this solution continues as a stationary solution even for large R.
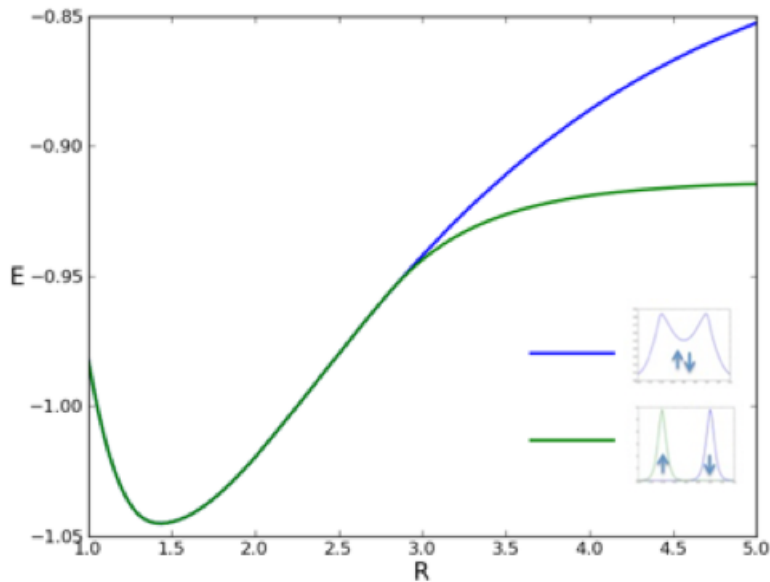

Figure 2: Bifurcation of LSDA for H_2 in the R dimension with $\alpha = 0.93$. The bifurcation point is at $R = 2.75$ au.

Note that the symmetry of total electron density is preserved in both the upper and lower states as in insert in Figure (2).

4.2.2 Hessian of bifurcated solutions for R variation

As discussed after the bifurcation illustrated in Figure 2 there are two solutions for $R > 2.75$ au. These (one spin localized/antiferomagnetic (green line) and one restricted (no localized spin) blue line) solutions are analogous to solution of spin ordered condensed systems and are widely interpreted in terms of the observed spin ordering of stable and unstable phases[26, 21, 49]. Since these solutions are remarkable stable in calculations, they can be difficult to identify on the basis of currently used optimization methods [26]. Typically several solutions may appear as stable in uncontrolled calculations. (For a brief overview of how spin is controlled in condensed matter calculations see reference [18].)

The stability/metastability of the solutions along the 2 branches In Figure (2) can be determined from the Hessian associated with the optimization problem Eq. (3) (see Appendix). At the bifurcation point, the gradient is zero. Numerical estimates of the eigenvalues of the Hessian the optimization problem Eq. (3) (also calculated via the FEM see appendix) show there is one negative eigenvalue for the RDFT solution beyond the bifurcation point. The combination of the zero gradient and the presence of the single negative eigenvalue shows that this is a metastable point in the energy surface. This is result may be important to DFT applications in which it is known that it is often difficult to find the true spin ordered minimum energy past the bifurcation point. This problem may be caused by the metastability of the delocalized state. We collect this information in a table for fixed $\alpha = .93$ (value consistent with the α typically used in DFT applications) varying the bond length in Table 1.

Bond Length	Solution	Result	Details
2.0 a.u.	delocalized solution	Local Minimizer	all evs on the constraint manifold > 0.
3.5+ a.u.	delocalized solution	Saddle Point	1 ev on the constraint manifold < 0.
3.5+ a.u.	localized solution	Local Minimizer	all evs on the constraint manifold > 0.

Table 1: Eigenvalues for the Hessian matrix, $\alpha = .93$ for various bond lengths

4.2.3 Bifurcation in the α dimension

Figure 3 shows the symmetry breaking bifurcation points for LSDA solutions of Eq. (refeq:LDA) with strength of the exchange contribution, α, for fixed bond lengths $R = 2.0$ au. As mentioned above adjustment of parameters such as α in the density functional formalism may improve DFT model performance for spin ordered systems [50, 26]. For a fixed bond length and in the small α domain, there are two identical degenerate spacial solutions (for spin up and spin down) degenerate solutions for the global minimum energy. These solutions (herein called the delocalized solutions) have peaks at the two atom centers, spread over the whole molecule and have the symmetry of the molecule. In this region, if a numerical solutions are initiated with broken symmetry the ψ_+ and ψ_- solutions evolve to have the same spacial dependance, $\psi_+ = \psi_-$. These solution are equivalent to the single orbital solution of of the restricted or doubly filled DFT product function. See the analysis in Section 2 for the demonstration of this result, but the underlying reason is that the Coulomb repulsion is somewhat insensitive to the localization of the total density and the kinetic energy dominates over the exchange potential contribution in Eq. (3). Beyond the bifurcation point (as illustrated in Figure (3), the broken symmetry solutions with excess spin on each atom (localized solutions) appears and the product solution is the global minimizer. The the total density still still has the symmetry of the molecule. The restricted solutions with higher energy still exists along the upper branch of the bifurcation curve. These solution have not been discussed above. Hessian analysis shows that delocalized solution is a metastable solution with Hessian eigenvalues demonstrating their metastable property similar to the bifurcation in R, Figure 2, namely there is one

negative eigenvalue for the RDFT solutions above the lowest energy curve (blue curve, Figure 2) beyond the bifurcation point.

As α is further increased (at constant R) a variety of new bifurcations appear. The exchange potential contributes much more than the Coulomb potential so the solution tends to be localized instead of delocalized. The localized solution (blue line Figure 3) remains the minimizer. The symmetric delocalized solution (dark green and light green Figure 3) is the highest energy. However for very high α the maximum density moves to the middle of the bond. For $\alpha > 6$ Figure 3 the high energy delocalized solutions break symmetry and forms two lower energy two electron solutions on centered on the atom centers (red line Figure 3). We note that the antiferromagnetic solution (blue line) is the global solution for all large α. This is an important result since this is the solution generally associated with magnetic behavior in real materials.
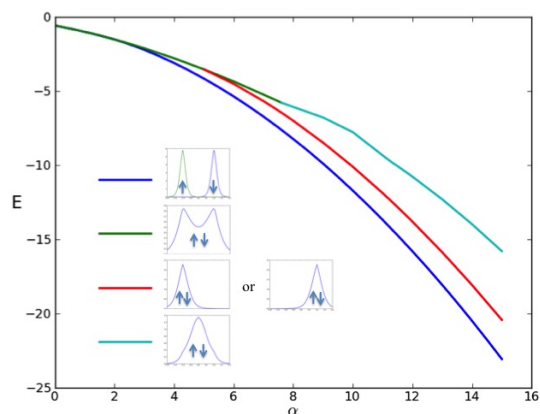

Figure 3: Several numerically constructed branches of the bifurcation of LSDA for H_2 in the α parameter with $R = 2.0$ au showing the relevant $\psi_\pm$ profiles.
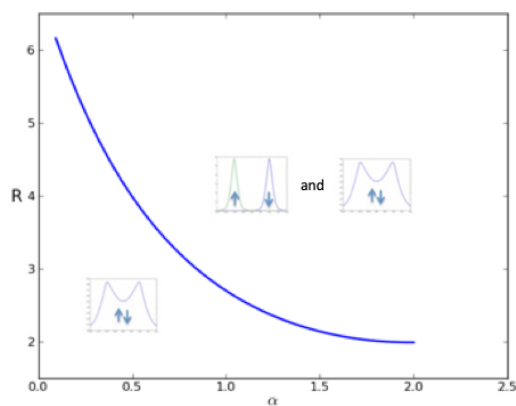

Figure 4: The first symmetry breaking bifurcation of LSDA for H_2 as a phase diagram in R and α. Below the line only delocalized states are present while above the line there are both delocalized and localized states.

4.2.4 Onset of ferromagnetic behavior as bond length is increased

Since the bond length corresponding to beginning of antiferromagnetic behavior (spin localization) occur after the first bifurcation and it is common to adjust the strength of the Dirac exchange to improve agreement of mode, we show the variation of the first bifurcation point for different α in Figure 4. Note that for very small α the bond length for bifurcation becomes very long.

5 Discussion and future works

A similar analysis to the large α case gives that the ground state Euler-Lagrange equation for large R can be transformed to an equation of the form

$$-\Delta\phi_\pm + R^2 E(R) - RV_1\phi_\pm + \frac{2}{R}\int \frac{|\phi_+|^2 + |\phi_-|^2}{|x-y|}\phi_\pm(x) + R\alpha|\phi_\pm|^{\frac{2}{3}}\phi_\pm = 0, \tag{62}$$

taking $\phi_\pm = R^{\frac{3}{2}}\psi_\pm$. This correlates to a new problem with no Coulomb repulsion, large but unit distance apart nuclear masses $Z = R$, and a very strong exchange-correlation nonlinearity $R\alpha$. Thus, the main issue is to study the nature of the stable curve for a large nuclear mass with strong exchange-correlation nonlinearity and observe what the nature of the Lagrange multiplier $R^2 E(R)$ should be as $R \to \infty$. The intuition is that this scales the problem to be localized since moving along the stable branch of states from low electron mass (small Lagrange multiplier) for the potential V_1 to large electron mass (large Lagrange multiplier) eventually concentrates onto localized states over each well. As the nonlinearity is growing in strength with the nuclear potential, this bifurcation onto localized modes will still happen at relatively low mass since after a scaling the model Lagrangian is

$$\frac{1}{2}\int |\nabla\phi|^2 dx + R\left(\int V_1|\phi|^2 dx - \alpha\int |\phi|^{\frac{8}{3}}dx\right), \quad \|\phi\|_{L^2} = 1, \tag{63}$$

meaning the behavior for large R should correlate to the mass 1 stability profile of the simplified (63).

Choosing $\phi_\pm = R^{\frac{3}{2}}\psi_\pm(Rx)$, the resulting modified Lagrangian has critical points given by

$$-\epsilon^2\Delta\phi_\pm + \phi_\pm - V_1\phi_\pm + \int \frac{|\phi_+|^2 + |\phi_-|^2}{|x-y|}\phi_\pm(x) + \alpha|\phi_\pm|^{\frac{2}{3}}\phi_\pm = 0, \tag{64}$$

which looks like a singular-perturbation Ginzburg-Landau style. As a result, this motivates the following question for a (strange) Hydrogen model: Is the minimizer of

$$E_H(u) = \frac{1}{2}\int |\nabla u|^2 \, dx - \int \frac{Z}{|x|}|u|^2(x) \, dx + \frac{1}{2}\iint \frac{|u|^2(x)|u|^2(y)}{|x-y|}\, dx\, dy - \int |u|^{8/3} dx \tag{65}$$

such that $\|u\|_{L^2} = 1$ orbitally stable. This has been answered in some sense when $Z = 0$ in [54] when the mass is that of the absolute minimizer. Understanding what occurs for the natural electronic mass 1 requires further investigation of this model and will be a topic of future work.

Acknowledgements

A   Appendix

We recall here the basics of the finite element methods we use in this work to numerically find critical points of the XLDA Lagrangian. The numerical algorithms are implemented using a *python* implementation of the FENICS finite element package, [22]. Many of the tools we use here are discussed in more detail in the works [16, 35]. For complete discussions of Finite Element Methods, see the books of [5, 9, 14, 6]. The method we develop here takes advantage of the sparsity of the FEM representation of the eigenvalue problem leading to an algorithm that scales linearly with number of basis functions. For resources on large scale computing in computational chemistry, see [36, 60].
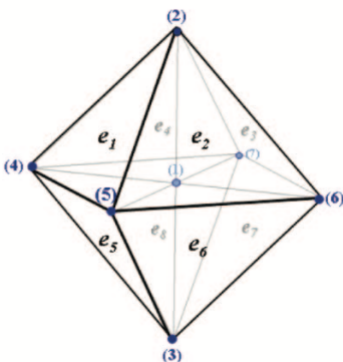
I. Finite Element Set Up

Figure 5: Finite element tetrahedron defining FEM elements and nodes. The L tetrahedral elements are identified by e_l. The global node are indexes by (m). For each element e_l a there is global node at each corner. Generally a local nodes belonging to individual tetrahedra are also defined. see [14, 5, 9, 16]. These are not shown and are managed transparently by the Dolfin software [44].

Assume that the solution, ϕ exists in a bounded domain $\Omega \in \mathscr{R}^3$ that can be divided into a set of L non overlapping tetrahedral elements, $\{e_l\}_{l=1}^{L}$ [14, 5, 9, 16], see Figures (5) and (1). For the electronic structure problems we are concerned with in this work the atomic potentials represented by $V(\vec{r})$ in the Hamlitonian below Eq. (71) are singular. This leads to rapid variation of the solution to the eigenvalue problem in this region. This requires that in order to obtain accuracy the FEM grid in this region must have a finer resolution as illustrated in Figure 1 and discussed in [17, 38, 16].

To construct the grid used in the calculation, we

1. Use BoxMesh to generate a coarse mesh in a $50 \times 50 \times 50$ domain. The initial number of cells in each direction is 2. So the total number of tetrahedra will be 48 and the total number of vertices will be 27 in the coarse mesh.

2. Find the closest mesh grids to the nuclei and set the parameter *cell_markers* true and use the refine function in DOLFIN [1, 16, 14, 5, 9] to refine the grids 20 times.

3. Refine the whole grids for 3 times.

Generally FEM nodes can be located at corners in along boundaries or in the centers of regions (tetrahedra) [14, 5, 9, 1]. However, for the calculations her nodes are located only at the corners of the tetrahedra. These nodes are shared by adjacent tetrahedra as in Figure (5). Each tetrahedral l has four corner nodes. A global index identifies a node as in Figure (5) (global node numbers in brackets). There are M global nodes in the construction. In actual calculations a local node index identifying a corner global

node with a basis function inside a particular tetrahedral is also defined in Dolfin[1, 16, 14, 5, 9] to identify variation associated with a node within a particular tetrahedra [14, 5, 9, 1]. The somewhat difficult book keeping problem of keeping track of the global variation of the basis functions consistent with their local behavior is taken care of nicely in the FEniCS software.[4]

For each node (with global index m and local index i) in a tetrahedral element, l, a finite element basis functions $\{\chi_i^{e_l}\}$ is defined. In these caculations the $\{\chi_i^{e_l}\}$ are linear functions centered on local nodes i in element e_l [1, 16, 14, 5, 9]. For each global node m the linear basis function $\{\chi_i^{e_l}\}$ is 1 on global node i and zero on all other nodes contained in the tetrahedrals containing global node m. For a particular tetrahedron the linear basis associated with local node i of tetrahedral e_l, $\{\chi_i^{e_l}\}$, has value only in tetrahedra e_l. Illustrations of how this works are given in [1]. The local node functions $\{\chi_i^{e_l}\}$ can be assembled in functions centered around the global nodes with index m as the global basis functions $\eta_m(\vec{r})$.

A piecewise continuous function (here the $\phi(\vec{x})$) can now be expanded as [16],

$$\phi(\vec{r}) = \sum_{m=1}^{M} c_m \eta_m(\vec{r}). \tag{66}$$

Here, M is the dimension of space of global nodes and c_m is the coefficient of basis element η_m. The value of the ψ_i on node i is c_m.

II. The Generalized Eigenvalue Problem:

With the above formulation, solving the Kohn-Sham minimization problem related to Eq. (3) leads to the generalized eigenvalue problem,

$$\mathbf{Hc} = \epsilon \mathbf{Sc}, \tag{67}$$

or more explicitly

$$H_{mn} c_{n,k} = \epsilon_k S_{mn} c_{n.k} \tag{68}$$

where k identifies the kth eigenfunction,

$$S_{mn} = \int_{\Omega} d\vec{r} \eta_m(\vec{r}) \eta_n(\vec{r}), \tag{69}$$

and

$$H_{mn} = \frac{1}{2} \int_{\Omega} d\vec{r} \nabla \eta_m(\vec{r}) \nabla \eta_n(\vec{r}) + \int_{\Omega} d\vec{r} \eta_m(\vec{r}) V_{\text{eff}} \eta_n(\vec{r}) \tag{70}$$

with V_{eff} given by

$$V_{\text{eff}} = V(\vec{r}) + V_{ee}(\rho) + V_{ex}(\rho, \alpha) = V(\vec{r}) + \int \frac{\rho(r')}{|\vec{r} - \vec{r'}|} d\vec{r'} + V_{ex}(\rho, \alpha). \tag{71}$$

Here $\rho(\vec{r})$ is the total electron density, $\left[\phi_+^2 + \phi_-^2 \right]$ and $V_{ex}(\rho, \alpha)$ is given by the scaled Dirac form studied above,

$$V_{ex}(\rho, \alpha) = \alpha \rho^{\frac{1}{3}}. \tag{72}$$

The matrix H_{mn}, Eq.(70), the overlap matrix S_{mn}, Eq. (69) and integrals over $V(\vec{r})$ in Eq. (71) can be obtained from the FEnics software [4]. The calculation of these matrix are also carefully discussed for electronic structure problem in ([16]) and in general in [14, 5, 9]. However, the full potential $V_{eff}(\rho)$ given by Eq. (71) is a function of the density requiring that the eigenvalue problem, Eq. (67), be solved iteratively to achieve self consistency.

III. Solution to the generalized eigenvalue problem and the associate Coulomb problem

The principle objective of the calculation is the solution of the generalized eigenvalue problem, Eq. (67). However, this 1st requires the input of a current estimate of the Classical potential V_{ee} required in V_{eff}, Eq. (71). This may be found as the solution to the Poisson equation

$$\nabla^2 V_{ee}(\vec{r}) = -4\pi \rho(\vec{r}) = -4\pi \sum_{i=1}^{N_e/2} |\phi_i(\vec{r})|^2. \tag{73}$$

To solve this pde $V_{ee}(\rho(\vec{(r)}))$ is also expanded in the finite element basis as,

$$V_{ee}(\vec{r}) = \sum_{m=1}^{M} v_m \eta_m(\vec{r}). \tag{74}$$

Eq. (73) is then discretized and reduced to a system of linear equations giving the $\{v_m\}$. Given a solution to the Coulomb problem, Eq. (73), based on a current density for the iteration, the generalized eigenvalue problem, Eq. (67) is also solved in the $\{\eta_m\}_{m=1}^{M}$ finite element basis functions. Each molecular orbital is represented as, (for this problem there is only one filled molecular orbital for each spin)

$$\phi_i = \sum_{\alpha=1}^{M} c_{im} \eta_m, i = 1, \ldots, n. \tag{75}$$

The finite element discretization of the one-electron equation for the current iteration is given as,

$$(T_i - \epsilon_i) c_i = v_i(\vec{r}). \tag{76}$$

$c_i = \{c_{i1}, \ldots, c_{im}\}$ are the coefficients of molecular orbital in the expansions of finite element basis. The elements of the operator $(T_i - \epsilon_i)$, are,

$$(T_i - \epsilon_i)_{mn} = \int_{\Omega} \left\{ \frac{1}{2} \nabla \eta_m \nabla \eta_n - \epsilon_i \eta_m \eta_n \right\} d\Omega. \tag{77}$$

The elements of v_i are,

$$(v_i)_m = \int \eta_m(\vec{r}) V_{\text{eff}}(\vec{r}) \phi_i(\vec{r}) d\Omega$$

$$= \int_{\Omega} \eta_m \left\{ V(\vec{r}) \phi_i(\vec{r}) - \int \frac{\left(|\phi_+(y)|^2 + |\phi_-(y)|^2 \right)}{|x - y|} dy \phi_i - \frac{4}{3} \alpha |\phi_i(x)|^{2/3} \phi_i \right\} d\Omega, \tag{78}$$

are calculated in an iterative process in which $V_{\text{eff}}(\vec{r})$ is defined for step k from the results of the self-consistent solver in the prior iteration.

Details of the FEniCS solver

The AMG is based on a V-cycle with a maximum number of multi grid levels of 25. For each fine to course grid transfer a single pre smoothing step is taken. For each course to fine transfer a single post smoothing step is taken. These smoothing steps use a symmetric-SOR/Jacobi method. On the coarsest level the course FEM equation is relaxed by Gaussian elimination. In the iteration an energy correction step is applied to update new eigenvalues after the Helmholtz equation is solved for a set of $\epsilon^{(k)}$ from the prior AMGCG cycle (see Appendix). The self-consistent solver converges when the total energy difference

in two consecutive iterations is smaller than a selected tolerance (see appendix). These are solved via the FEniCs code using the GMRES [56] and BOOMER AMG (Algebraic Multigrid [15]) packages. The solution to this problem is of order M [35].

Eq. (76) or (77) can be solved in $O(m)$ steps using the FEniCS software [4] The solution to Eq. (77) is can be solved by general minimal residue method (GMRES) [56] using the FEniCS software. To improve the convergence of the solution to a preconditioning based on the algebraic multigrid method is used [59, 61]. For an introduction to multigrid methods and their application to problems in electronic structure, see [17, 38, 15, 10, 11, 13, 12, 32, 33, 45].

IV. The Wavefunction and Orbital Energy update and iteration

IV.i: Some Preliminaries

The eigenvalue problem is solved using an iterative process in which for step k the ϕ_{pm} on right hand side of Eq. (76) and the orbital energies, $\epsilon_{\pm}^{(k)}$, at step k are assigned the the values and functionality from the $k-1$ step The iteration is developed with the intention of producing linear scaling in the number of FEL basis functions m. We note that *scaling in the number of electrons (n) is typically higher.* This is achieved by developing a solver strategy that emphasizes the use of the operator $(\nabla^2 - k^2)$ which is easily implemented in multigrid schemes.

The density functional equations at iteration k are written as

$$\left[-\frac{1}{2}\nabla_{\vec{r}}^2 - \epsilon_i\right]\phi_i^{(k+1)}(\vec{r}) = \left[V_{ext}(\vec{r}) + V_{ee}(\rho^{(k)}(\vec{r}) + V_{ex}(\rho^{(k)}(\vec{r}))\right]\phi_i^{(k)}(\vec{r}) \tag{79}$$

Here n is the number of filled electron states and V_i^{ext} is the external potential. The Coulomb potential (calculated from FeniCS as above) is defined by

$$V_{ee}(\vec{r}) = \int \frac{\phi_j^{(k)}(\vec{r'})\phi_j^{(k)}(\vec{r'})}{\left|\vec{r} - \vec{r'}\right|}d\vec{r'}. \tag{80}$$

The exchange potential is given by

$$V_{ex}(\vec{r}) = \alpha\rho^{(k)}(\vec{r})^{\frac{1}{3}}. \tag{81}$$

In this work we developed a multigrid based solver that captures the efficiency of the sparsity of the FEM representation of the eigenvalue problem.
The point here is that this is now a linear PDE of the form

$$\left[-\frac{1}{2}\nabla_{\vec{r}}^2 - \epsilon_i^{(k-1)}\right]\phi_i^{(k)}(\vec{r}) = f_i^{(k-1)}(\vec{r}) \tag{82}$$

We now calculate the solution to this equation using an efficient multigrid method. Because of the complexity of the grid we use the AMGCG implemented in the FEniCS software [4]. At this point we have an equation that efficiently updates $\phi_i^{(k-1)}$ to $\phi_i^{(k)}$. But for a full update we need $\epsilon^{(k)}$. To obtain the energy update Houdong introduced two methods. The most straightforward is to use the updated $\phi_i^{(k)}$ to diagonalize the Fock matrix. A second method develops an iterative solution.

IV.ii: Update of the wavefunction, $\phi_i(\vec{x})$:

Suppose we have solutions $\phi_i^{(k-1)}(\vec{x})$ and $\epsilon_i^{(k-1)}$. The update of $\phi_i^{(k-1)}(\vec{x})$ to $\phi_i^{(k)}(\vec{x})$ proceeds directly from

$$\phi_i^{(k)}(\vec{x}) = \left[-\frac{1}{2}\nabla_{\vec{x}}^2 - \epsilon_i^{(k-1)} \right]^{-1} f_i^{(k-1)}(\vec{x}). \tag{83}$$

All the functions in this equation are defined. Indeed, this is the solution that we obtain from AMGCG. This then is the update of the wave function from $\phi_i^{(k-1)}(\vec{x})$ to $\phi_i^{(k)}(\vec{x})$, which we will sometimes refer to $\tilde{\phi}_i^{(k)}(\vec{x})$ below. Now we also need an update of the orbital energy.

IV.iii: Update of the orbital energy:

Again we assume we have $\phi_i^{(k-1)}(\vec{x})$ and $\epsilon_i^{(k-1)}$. Keep in mind that we obtained $\phi_i^{(k-1)}(\vec{x})$ from an AMGCG upgrade using the potentials $f_i^{(k-2)}(\vec{x})$. We begin by defining two Greens functions (propagators): The $(k-1)$ Green's function, $G_i^{(k-1)}$, with energy $\epsilon^{(k-1)}$:

$$G_i^{(k-1)} = \left\{ -\frac{1}{2}\nabla^2 - \epsilon_i^{(k-1)} \right\}^{-1} \tag{84}$$

and a Green's function, G_i^{con} with the converged HF orbital energy, ϵ_i^{con},

$$\epsilon_i^{con} = (\epsilon_i^{(k-1)} + \delta\epsilon_i^{(k-1)}) \tag{85}$$

giving

$$G_i^{con} = \left\{ -\frac{1}{2}\nabla^2 - \epsilon_i \right\}^{-1} = \left\{ \frac{1}{2}\nabla^2 - (\epsilon_i^{(k-1)} + \delta\epsilon_i^{(k-1)}) \right\}^{-1} \tag{86}$$

the objective is to calculate an orbital energy correction from these equations.

Suppose that $\phi_i^{(k-1)}$ is a good approximation to the converged HF orbital ϕ_i^{con}. ϕ_i^{con} satisfies the Fock orbital PDE with solution,

$$\phi_i^{con}(\vec{x}) = \left\{ -\frac{1}{2}\nabla^2 - \epsilon_i^{con} \right\}^{-1} f_i^{con}(\vec{x}). \tag{87}$$

In this equation ϵ_i^{con} is the converged orbital energy. We also define $\delta\epsilon_i^{(k-1)}$ (*the energy update*) by

$$\epsilon_i^{con} = \epsilon_i^{(k-1)} + \delta\epsilon_i^{(k-1)} \tag{88}$$

$\phi^{(k-1)}$ is a good approximation to ϕ_i^{con}. That means it approximately satisfies,

$$\phi_i^{(k-1)}(\vec{x}) = \left\{ -\frac{1}{2}\nabla^2 - \epsilon_i \right\}^{-1} f i_i^{(k-1)}(\vec{x}) = \left\{ -\frac{1}{2}\nabla^2 - (\epsilon_i^{(k-1)} + \delta\epsilon_i^{(k-1)}) \right\}^{-1} f^{(k-1)}(\vec{x}) \tag{89}$$

Now we need to expand the full Greens function (RHS) in the energy correction $\delta\epsilon_I^{(k-1)}$ to obtain an equation that will update the orbital energy (find an optimal correction to $\epsilon_i^{(k-1)}$).

Now we use the operator identity

$$\frac{1}{(1+a+b)} = \frac{1}{(1+a)} + \frac{1}{(1+a)}\frac{-b}{(1+a+b)}. \tag{90}$$

Using in the full propagator we obtain (reproduced from above for completeness)

$$\left\{-\frac{1}{2}\nabla^2 - \epsilon_i^{(k-1)} - \delta\epsilon_i^{(k-1)}\right\}^{-1} = \left\{-\frac{1}{2}\nabla^2 - \epsilon_i^{(k-1)}\right\}^{-1} - \left[\left\{-\frac{1}{2}\nabla^2 - \epsilon_i^{(k-1)}\right\}^{-1}\right.$$
$$\left.\left\{-\delta\epsilon_i^{(k-1)}\right\}\left\{-\frac{1}{2}\nabla^2 - \epsilon_i^{(k-1)} - \delta\epsilon_i^{(k-1)}\right\}^{-1}\right].$$
(91)

Iteration of this equation to obtain an expression for the propagator to 1st order in the number $\delta\epsilon_i^{(k-1)}$ we obtain,

$$\left\{-\frac{1}{2}\nabla^2 - \epsilon_i^{(k-1)} - \delta\epsilon_i^{(k-1)}\right\}^{-1} = \left\{-\frac{1}{2}\nabla^2 - \epsilon_i^{(k-1)}\right\}^{-1} - \left[\left\{-\frac{1}{2}\nabla^2 - \epsilon_i^{(k-1)}\right\}^{-1}\right.$$
$$\left.\times \left\{\delta\epsilon_i^{(k-1)}\right\}\left\{-\frac{1}{2}\nabla^2 - \epsilon_i^{(k-1)}\right\}^{-1}\right].$$
(92)

Now we can use this result in Eq. (89) to obtain,

$$\phi_i^{(k-1)}(\vec{x}) = \left\{-\frac{1}{2}\nabla^2 - \epsilon^{(k-1)}\right\}^{-1} f_i^{(k-1)}(\vec{x})$$
$$- \left\{-\frac{1}{2}\nabla^2 - \epsilon^{(k-1)}\right\}^{-1} \delta\epsilon^{(k-1)} \left\{-\frac{1}{2}\nabla^2 - \epsilon^{(k-1)}\right\}^{-1} f_i^{(k-1)}(\vec{x}).$$
(93)

In vector notation this is,

$$\left|\phi_i^{(k-1)}(\vec{x})\right\rangle = \left\{-\frac{1}{2}\nabla^2 - \epsilon^{(k-1)}\right\}^{-1} \left|f_i^{(k-1)}\right\rangle$$
$$- \left\{-\frac{1}{2}\nabla^2 - \epsilon^{(k-1)}\right\}^{-1} \delta\epsilon_i^{(k-1)} \left\{-\frac{1}{2}\nabla^2 - \epsilon^{(k-1)}\right\}^{-1} |f_i^{(k-1)}\rangle$$
(94)

or

$$0 = -\left|\phi_i^{(k-1)}\right\rangle + \left\{-\frac{1}{2}\nabla^2 - \epsilon^{(k-1)}\right\}^{-1} \left|f_i^{(k-1)}\right\rangle$$
$$- \left\{-\frac{1}{2}\nabla^2 - \epsilon^{(k-1)}\right\}^{-1} \delta\epsilon_i^{(k-1)} \left\{-\frac{1}{2}\nabla^2 - \epsilon^{(k-1)}\right\}^{-1} |f_i^{(k-1)}\rangle.$$
(95)

Closing this equation on the left with $\left\langle f^{(k-1)}\right|$ gives a linear expression for $\delta\epsilon_i^{(k-1)}$ which may be in terms of the $\tilde{\phi}_i^{(k-1)}$ as,

$$0 = -\left\langle f_i^{(k-1)} \middle| \phi_i^{(k-1)} \right\rangle + \left\langle f^{(k-1)i} \middle| \tilde{\phi}_i^{(k-1)} \right\rangle$$
$$- \delta\epsilon_i^{(k-1)} || \left\langle \tilde{\phi}^{(k-1)i} \middle| \tilde{\phi}_i^{(k-1)} \right\rangle ||^2.$$
(96)

This may be solved for $\delta\epsilon_i^{(k-1)}$ to obtain

$$\delta\epsilon_i^{(k-1)} = \frac{-\left\langle f_i^{(k-1)} \middle| \phi_i^{(k-1)} \right\rangle + \left\langle f^{(k-1)i} \middle| \tilde{\phi}_i^{(k-1)} \right\rangle}{|| \left\langle \tilde{\phi}^{(k-1)i} \middle| \tilde{\phi}_i^{(k-1)} \right\rangle ||^2}.$$
(97)

This is essentially Eq. (4.4.10) in [35] and the equation we use in our iteration.

V. The Self Consistent Iteration

Algorithm 1 shows the process of the self-consistent solver. An initial guess $(c_i^{(0)}, \epsilon_i^{(0)}), i = 1, \ldots, n$ is given to start the self-consistent solver. The self-consistent solver will stop when the total energy difference in two consecutive iterations is smaller than the tolerance TOL.

Algorithm 1 The Self-consistent Iteration

Input $(c_i^{(0)}, \epsilon_i^{(0)}), i = 1, \ldots, n$, TOL;
while $\|\epsilon_{total}^{(k)} - \epsilon_{total}^{(k-1)}\| > $TOL **do**
    Evaluate potentials $V_{ij}^{(k)}, i, j = 1, \ldots, n$;
    Evaluate $v_i^{(k)}(\vec{x}), i = 1, \ldots, n$;
    Solve Helmholtz equation, and get updated $\{c_i^{(k+1)}, i = 1, \ldots, n\}$;
    energy correction step, and get updated $\{\epsilon_i^{(k+1)}, i = 1, \ldots, n\}$;
    k++;
Output $(c_i, \epsilon_i), i = 1, \ldots, n$.

VI. Hessian analysis

The unrestricted density functional theory for two-electrons' system has two orbital wavefunctions (ψ_+, ψ_-). The model we discussed below is local spin density approximation without correlation energy functional. Total energy functional is $E(\psi)$ is

$$E_\alpha(\psi_+, \psi_-) = \frac{1}{2}\int \left|\nabla\psi_+\right|^2 \mathrm{d}x + \frac{1}{2}\int \left|\nabla\psi_-\right|^2 \mathrm{d}x + \int V_R(x)\left(\left|\psi_+(x)\right|^2 + \left|\psi_-(x)\right|^2\right)\mathrm{d}x$$
$$+ \frac{1}{2}\iint \frac{\left(\left|\psi_+(x)\right|^2 + \left|\psi_-(x)\right|^2\right)\left(\left|\psi_+(y)\right|^2 + \left|\psi_-(y)\right|^2\right)}{\left|x - y\right|}\mathrm{d}x\,\mathrm{d}y - \alpha\int\left(\left|\psi_+(x)\right|^{8/3} + \left|\psi_-(x)\right|^{8/3}\right)\mathrm{d}x, \quad (98)$$

where $V_R(x)$ is the nuclear potential. The constraints on (ψ_+, ψ_-) are

$$\int \left|\psi_i(x)\right|^2 \mathrm{d}x = 1, i = +, -. \tag{99}$$

By Lagrange multiplier method, we have

$$L(\psi_+, \psi_-, \epsilon_+, \epsilon_-) = \frac{1}{2}\int \left|\nabla\psi_+\right|^2 \mathrm{d}x + \frac{1}{2}\int \left|\nabla\psi_-\right|^2 \mathrm{d}x + \int V_R(x)\left(\left|\psi_+(x)\right|^2 + \left|\psi_-(x)\right|^2\right)\mathrm{d}x$$
$$+ \frac{1}{2}\iint \frac{\left(\left|\psi_+(x)\right|^2 + \left|\psi_-(x)\right|^2\right)\left(\left|\psi_+(y)\right|^2 + \left|\psi_-(y)\right|^2\right)}{\left|x - y\right|}\mathrm{d}x\,\mathrm{d}y - \alpha\int\left(\left|\psi_+(x)\right|^{8/3} + \left|\psi_-(x)\right|^{8/3}\right)\mathrm{d}x$$
$$- \epsilon_+\left(\int \left|\psi_+(x)\right|^2 \mathrm{d}x - 1\right) - \epsilon_-\left(\int \left|\psi_-(x)\right|^2 \mathrm{d}x - 1\right), \quad (100)$$

where (ϵ_+, ϵ_-) are the Lagrange multipliers.

Using the Euler-Lagrange equations of the total energy functional with the constraints, which are the effective one-electron eigenvalue equations, we can calculate the extremum of $L(\psi, \epsilon)$

$$\frac{\delta L}{\delta \psi_i} = 0 \Rightarrow \left(-\frac{1}{2}\nabla^2 + V_R(x) + \int \frac{\left(\left|\phi_+(y)\right|^2 + \left|\phi_-(y)\right|^2\right)}{\left|x - y\right|}\mathrm{d}y - \frac{4}{3}\alpha\left|\phi_i(x)\right|^{2/3}\right)\phi_i(x) = \varepsilon_i\phi_i(x), i = +, -, \quad (101)$$

where (ψ_+, ψ_-) and $(\varepsilon_+, \varepsilon_-)$ are the solutions that satisfy the constraints (101).

In order to determine whether an extremum is a maximizer, minimizer or saddle point, the second order functional derivative (Hessian matrix) has to be analyzed. Suppose the extremum (ϕ_+, ϕ_-) and $(\varepsilon_+, \varepsilon_-)$ satisfy both (101) and (99) and (λ_i, w_i) are eigenvalues and eigenvectors of **Hess** respectively, the Hessian analysis involves the solutions of the eigenvalue problems

$$\mathbf{Hess}\, w_i(y) = \int \frac{\delta L(\psi, \epsilon)}{\delta \psi_i(x)\delta\psi_j(y)} w_i(y)\, \mathrm{d}y \bigg|_{(\psi,\epsilon)=(\phi,\epsilon)} = \lambda_i\, w_i(x), i = +, -, \tag{102}$$

which lead to the Hessian matrix

$$\mathbf{Hess} = \begin{pmatrix} H_{11} & \int \dfrac{2\phi_-(y)}{|x-y|}\mathrm{d}y\,\phi_+(x) \\ \int \dfrac{2\phi_+(y)}{|x-y|}\mathrm{d}y\,\phi_-(x) & H_{22} \end{pmatrix} \tag{103}$$

where

$$H_{11} = -\tfrac{1}{2}\nabla^2 + V_R + \int \frac{|\phi_-(y)|^2}{|x-y|}\mathrm{d}y - \tfrac{20}{9}\alpha|\phi_+(x)|^{2/3} - \varepsilon_+,$$

$$H_{22} = -\tfrac{1}{2}\nabla^2 + V_R + \int \frac{|\phi_+(y)|^2}{|x-y|}\mathrm{d}y - \tfrac{20}{9}\alpha(|\phi_-(x)|^{2/3} - \varepsilon_-.$$

and w_i need to satisfy the constraints

$$\int \phi_i(x)w_i(x)\,\mathrm{d}x = 0, i = +, - \tag{104}$$

meaning that w_i are orthonormal to ϕ_i.

References

[1] Finite element basis functions(1). hplgit.github.io.

[2] Hypre library.

[3] Arnaud Anantharaman and Eric Cancès. Existence of minimizers for Kohn–Sham models in quantum chemistry. 26(6):2425–2455, 2009.

[4] Garth N. Wells Anders Logg, Kent-Andre Mardel, editor. *Automated Solution of Differential Equations by the Finite Element method: The FEniCS Book.* Springer, 2012.

[5] O. Axelsson and V. A. Barker. *Finite Element Solution of Boundary Value Problems: Theory and Computation.* SIAM, 2001.

[6] Randolph E Bank and Todd Dupont. An optimal order process for solving finite element equations. *Mathematics of Computation*, 36(153):35–51, 1981.

[7] Giuseppe M. J. Barca, Andrew T. B. Gilbert, and Peter M. W. Gill. Communication: Hartree-Fock description of excited states of H2. *The Journal of chemical physics*, 141(11):111104, 2014.

[8] Rafael Benguria, Haïm Brézis, and Elliott H Lieb. The thomas-Fermi-von Weizsäcker theory of atoms and molecules. *Communications in Mathematical Physics*, 79(2):167–180, 1981.

[9] Dietrich Braess. *Finite elements: theory, fast solvers and applications in solid mechanics, second edition.* Cambridge University Press, 2001.

[10] James H Bramble. *Multigrid methods*, volume 294. CRC Press, 1993.

[11] James H Bramble and Joseph E Pasciak. New convergence estimates for multigrid algorithms. *Mathematics of computation*, 49(180):311–329, 1987.

[12] A Brandt, S McCoruick, and J Huge. Algebraic multigrid (amg) f0r sparse matrix equati0ns. *Sparsity and its Applications*, page 257, 1985.

[13] Achi Brandt. Algebraic multigrid theory: The symmetric case. *Applied mathematics and computation*, 19(1):23–56, 1986.

[14] Susanne C Brenner and Larkin Ridgway Scott. *The mathematical theory of finite element methods*, volume 15. Springer, 2008.

[15] William L Briggs, Van Emden Henson, and Steve F McCormick. *A multigrid tutorial: second edition.* SIAM, 2000.

[16] Eric J Bylaska, Michael Holst, and John H Weare. Adaptive finite element method for solving the exact kohn- sham equation of density functional theory. *Journal of Chemical Theory and Computation*, 5(4):937–948, 2009.

[17] Eric J Bylaska, Scott R Kohn, Scott B Baden, Alan Edelman, Ryoichi Kawai, M Elizabeth G Ong, and John H Weare. Scalable parallel numerical methods and software tools for material design. *Proceedings of the Seventh SIAM Conference on Parallel Processing for Scientific Computing*, pages 219–224, 1995.

[18] Ying Chen, Eric Bylaska, and John Weare. First principles estimation of geochemically important transition metal oxide properties. In James D. Kubicki, editor, *Molecular Modeling of Geochemical Reactions*, chapter 4. Wiley, 2016.

[19] A. J. Cohen, P. Mori-Sánchez, and W. Yang. Insights into current limitations of density functional theory. *Science*, 321:792 – 794, 2008.

[20] A. J. Cohen, P. Mori-Sánchez, and W. Yang. Challenges for density functional theory. *Chem. Rev.*, 112:289–320, 2012.

[21] P. A. Cox. *Transition Metal Oxides*. Clearendon Press, Oxford, 1992.

[22] Todd Dupont, Johan Hoffman, Claus Johnson, Robert C Kirby, Mats G Larson, Anders Logg, and L Ridgway Scott. *The FEniCS project*. Chalmers Finite Element Centre, Chalmers University of Technology, 2003.

[23] James B. Foresman and AEleen Frisch. *Exploring Chemistry with Electronic Structure Methods*. Gaussian, 1996.

[24] Rupert L Frank, Elliott H Lieb, Robert Seiringer, and Lawrence E Thomas. Bipolaron and n-polaron binding energies. *Physical review letters*, 104(21):210402, 2010.

[25] Rupert L Frank, Elliott H Lieb, Robert Seiringer, and Lawrence E Thomas. Stability and absence of binding for multi-polaron systems. *Publications mathématiques de l'IHÉS*, 113(1):39–67, 2011.

[26] P. Engel G. Rollmann, A. Rohrbach and J. Haftner. First-principle calculations of the structure and magnetic properties of hematite. *Physical Review B*, 69:165107 1–12, 2004.

[27] Gene H. Golub. *Matrix Computations*. Johns Hopkins Press, 1996.

[28] David Gontier. Existence of minimizers for Kohn–Sham within the local spin density approximation. *Nonlinearity*, 28(1):57, 2015.

[29] David Gontier, Christian Hainzl, and Mathieu Lewin. Lower bound on the hartree-fock energy of the electron gas. *arXiv preprint arXiv:1811.12461*, 2018.

[30] David Gontier and Mathieu Lewin. Spin symmetry breaking in the translation-invariant hartree-fock uniform electron gas. *arXiv preprint arXiv:1812.07679*, 2018.

[31] Marcel Griesemer and Fabian Hantsch. Unique solutions to Hartree–Fock equations for closed shell atoms. *Arch. Rational Mech. Anal.*, 203(3):883–900, 2012.

[32] Wolfgang Hackbusch. *Multi-grid methods and applications*, volume 4. Springer-Verlag Berlin, 1985.

[33] Robert J Harrison, George I Fann, Takeshi Yanai, Zhengting Gan, and Gregory Beylkin. Multiresolution quantum chemistry: Basic theory and initial applications. *The Journal of chemical physics*, 121(23):11587–11598, 2004.

[34] Warren J Hehre, Robert F Stewart, and John A Pople. self-consistent molecular-orbital methods. i. use of gaussian expansions of slater-type atomic orbitals. *The Journal of Chemical Physics*, 51(6):2657–2664, 1969.

[35] Houdong Hu. Electronic structure models: Solution theory, linear scaling methods, and stability analysis. *UCSD Ph.D. Thesis*, 2014.

[36] Ricky A Kendall, Edoardo Aprà, David E Bernholdt, Eric J Bylaska, Michel Dupuis, George I Fann, Robert J Harrison, Jialin Ju, Jeffrey A Nichols, Jarek Nieplocha, et al. High performance computational chemistry: An overview of nwchem a distributed parallel application. *Computer Physics Communications*, 128(1):260–283, 2000.

[37] E. Kirr, P. G. Kevrekidis, and D. E. Pelinovsky. Symmetry-breaking bifurcation in the nonlinear Schrödinger equation with symmetric potentials. *Communications in mathematical physics*, 308(3):795–844, 2011.

[38] Scott R Kohn, John H Weare, M Elizabeth G Ong, and Scott B Baden. Parallel adaptive mesh refinement for electronic structure calculations. *Proceedings of the Eighth SIAM Conference on Parallel Processing for Scientific Computing*, 1997.

[39] E. Lenzmann. Uniqueness of ground states for pseudorelativistic Hartree equations. *Analysis & PDE*, 2(1):1–27, 2009.

[40] E. H. Lieb and M. Loss. *Analysis*. American Mathematical Society, 2nd edition, 2001.

[41] Elliott H Lieb. Thomas-Fermi and related theories of atoms and molecules. *Reviews of Modern Physics*, 53(4):603, 1981.

[42] Elliott H Lieb and Barry Simon. The Hartree-Fock theory for Coulomb systems. *Communications in Mathematical Physics*, 53(3):185–194, 1977.

[43] Pierre-Louis Lions. Solutions of Hartree-Fock equations for Coulomb systems. *Communications in Mathematical Physics*, 109(1):33–97, 1987.

[44] Anders Logg and Garth N. Wells. Dolfin: Automated finite element computing. *ACM Transations on Mathematical Software (TOMS)*, 37(issue 2, article 20), 2010.

[45] Stephen F McCormick. *Multigrid methods*, volume 3. SIAM, 1987.

[46] G. L. Oliver and J. P. Perdew. Spin-density gradient expansion for kinetic energy. *Physical Review A*, 20(2):397–403, 1979.

[47] Robert G. Parr. *Quantum Theory of Molecular Electronic Structure*. W. A. Benjamin, 1972.

[48] Robert G. Parr and Weitao Yang. *Density-Functional Theory of Atoms and Molecules*. Oxford Science Publications, 1989.

[49] Haowei Peng and John P. Perdew. Synergy of van der waals and self-interaction corrections in transition metal monoxides. *Physical Review B*, 96:100101 1–5, 2017.

[50] Z.D. Pozan and Graeme Henkelman. Hybrid density functional theory band structure engineering in hematite. *The Journal of Chemical Physics*, 134:224706–1–9, 2011.

[51] Michael Reed and Barry Simon. *Analysis of Operators, Vol. IV of Methods of Modern Mathematical Physics*. New York, Academic Press, 1978.

[52] Julien Ricaud. *Symétrie et brisure de symétrie pour certains problèmes non linéaires*. PhD thesis, Université de Cergy Pontoise, 2017.

[53] Julien Ricaud. Symmetry breaking in the periodic thomas–fermi–dirac–von weizsäcker model. In *Annales Henri Poincaré*, volume 19, pages 3129–3177. Springer, 2018.

[54] David Ruiz. On the Schrödinger–Poisson–Slater system: behavior of minimizers, radial and nonradial cases. *Archive for rational mechanics and analysis*, 198(1):349–368, 2010.

[55] Mary Beth Ruskai and Frank H Stillinger. Binding limit in the Hartree approximation. *J. Math. Phys.*, 25(6):2099–2103, 1984.

[56] Youcef Saad and Martin H. Schultz. Gmres: A generalized minimal residual algorithm for solving nonsymmetric linear systems. *SIAM J. Sci. Stat. Comput.*, 7(3):856âĂŞ869, 1986.

[57] Catherine Sulem and Pierre-Louis Sulem. *The nonlinear Schrödinger equation: self-focusing and wave collapse*, volume 139. Springer Science & Business Media, 1999.

[58] Attila Szabo and Neil S. Ostlund. *Modern Quantum Chemistry*. Dover Publications, 1989.

[59] Osamu Tatebe. The multigrid preconditioned conjugate gradient method, 1993.

[60] Marat Valiev and et al. Nwchem: a comprehensive and scalable open-source solution for large scale molecular simulations. *Computer Physics Communications*, 181(9):1477–1489, 2010.

[61] Henson Van Emden and Ulrike Meir Yang. Boomer amg: A parallel algebraic multigrid solver and preconditioner. *Applied Numerical Mathematics*, 41:155–177, 2002.

[62] Michael I Weinstein. Lyapunov stability of ground states of nonlinear dispersive evolution equations. *Communications on Pure and Applied Mathematics*, 39(1):51–67, 1986.